

JANUARY 2019

M.Sc. in Engineering Physics

NURETTİN GÖKDENİZ

UNIVERSITY OF GAZİANTEP  
GRADUATE SCHOOL OF  
NATURAL & APPLIED SCIENCES

MODELLING OF NOVEL BISMIDE ALLOYS FOR  
OPTOELECTRONIC DEVICES

M.Sc. THESIS  
IN  
ENGINEERING PHYSICS

BY  
NURETTİN GÖKDENİZ

JANUARY 2019

**Modelling of Novel Bismide Alloys for  
Optoelectronic Devices**

**M.Sc. Thesis  
in  
Engineering Physics  
University of Gaziantep**

**Major Supervisor  
Prof. Dr. Beşire GÖNÜL**

**Co-Supervisor  
Asst. Prof. Dr. Ömer Lütfi ÜNSAL**

**By  
Nurettin GÖKDENİZ**

**January 2019**

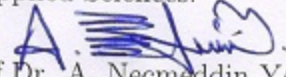


© 2019 [NURETTİN GÖKDENİZ]


REPUBLIC OF TURKEY  
GAZIANTEP UNIVERSITY  
GRADUATE SCHOOL OF  
NATURAL AND APPLIED SCIENCES  
ENGINEERING PHYSICS

Name of the Thesis : Modelling of Novel Bismide Alloys for Optoelectronic  
Devices  
Name of the Student : Nurettin Gökdeniz  
Exam Date : 02.01.2019

Approval of the Graduate School of Natural and Applied Sciences.

  
Prof. Dr. A. Necmeddin YAZICI  
Director

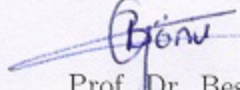
I certify that this thesis satisfies all the requirements as a thesis for the degree of  
Master of Science.

  
Prof. Dr. Ramazan KOÇ  
Head of Department

This is to certify that we have read this thesis and that in our opinion it is fully  
adequate, in scope and quality, as a thesis for the degree of Master of Science.

Asst. Prof. Dr. Ömer Lütfi ÜNSAL  
Co-Supervisor



  
Prof. Dr. Beşire GÖNÜL  
Major Supervisor

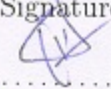
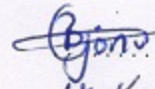
Examining Committee Members:

Prof. Dr. Mustafa ÖZTAŞ

Prof. Dr. Beşire GÖNÜL

Assoc. Prof. Dr. Vural Emir KAFADAR

Signature

  
.....  
  
.....  
Dr. Kafadar

I hereby declare that all information in this document has been obtained and presented in accordance with academic rules and ethical conduct. I also declare that, as required by these rules and conduct, I have fully cited and referenced all material and results that are not original to this work.

Nurettin GÖKDENİZ

## ABSTRACT

### MODELLING OF NOVEL BISMIDE ALLOYS FOR OPTOELECTRONIC DEVICES

GÖKDENİZ, Nurettin

M.Sc. in Engineering Physics

Major Supervisor: Prof. Dr. Beşire GÖNÜL

Co-Supervisor: Asst. Prof. Dr. Ömer Lütfi ÜNSAL

January 2019

68 pages

The purpose of this thesis work is to investigate the electronic band structures of InAsBi/InAs, InPBi/InP, InSbBi/InSb and GaAsBiN/GaAs III-V materials by means of using model calculations. When bismuth and nitrogen atoms are incorporated into a III-V binary host semiconductor, bismuth and nitrogen impurity atoms occupy at localized energy levels which lies inside or close to the valence and conduction band, respectively. These localized impurity states interact with the extended valence and conduction band states of host alloy. This interaction causes a splitting in each of these band states of the light hole, heavy-hole, split-off band and conduction subbands into subbands of  $E_+$  and  $E_-$  energy levels. The incorporation of dilute bismides and nitrides into host materials cause a reduction in band gap with increasing bismuth and nitrogen concentration, an increase in spin-orbit splitting energy with increasing bismuth concentration. These major modifications in band structure tends to eliminate or suppress optical loss mechanism, such as Auger recombination and Intervalence band absorption.

Our theoretical analysis is based on the conduction band anti-crossing, C-BAC, model for incorporation of dilute nitrides and the valence band anti-crossing, V-BAC, model for incorporation of dilute bismides to model the restructuring of valence and conduction bands.

**Key words:** Electronic band structure, strain, dilute bismides, dilute nitrides, band anti-crossing model, band gap energy, spin-orbit-splitting energy

## ÖZET

### OPTOELEKTRONİK CİHAZLAR İÇİN BİZMUT ALAŞIMLARININ MODELLENMESİ

GÖKDENİZ, Nurettin

Yüksek Lisans Tezi, Fizik Mühendisliği

Tez Yöneticisi: Prof. Dr. Beşire GÖNÜL

Tez Yönetici Yardımcısı: Dr. Öğr Üyesi Ömer Lütfi ÜNSAL

Ocak 2019

68 sayfa

Bu tez çalışmasının amacı, InAsBi/InAs, InPBi/InP, InSbBi/InSb ve GaAsBiN/-GaAs III-V malzemelerinin elektronik bant yapılarını model hesaplamaları kullanarak incelemektir. Bizmut ve nitrojen atomları bir III-V ikili yarı iletkenine eklendiğinde, katkı atomları bizmut ve nitrojen atomları iletkenlik bandı ve değerlik bandına yakın yerlerde bulunan enerji seviyelerini işgal eder. Bu lokalize katkı atomları iletkenlik bandı ve değerlik bandı ile etkileşime girer. Bu etkileşim sonucu değerlik bandı ve iletkenlik bandı pozitif ve negatif enerji seviyelerine ayrılır, değerlik bandı hafif boşluk, ağır boşluk, spin-off ve iletkenlik bandı ise alt bantlarına ayrılır. Seyreltik bismutların ve nitritlerin ikili ev sahibi maddelere eklenmesi sonucu, bizmut ve nitrojen konsantrasyonunun artması, bant boşluğu enerjisinde bir azalmaya neden olur. Ayrıca bizmut konsantrasyonunun artmasıyla birlikte spin yörünge etkileşim enerjisinde bir artış olur. Bant yapısındaki bu büyük değişiklikler, Auger rekombinasyonu ve Intervalence bant absorpsiyonu gibi optik kayıp mekanizmalarını ortadan kaldırmaya veya bastırmaya eğilimlidir.

Teorik analizimiz, değerlik ve iletkenlik bantlarının yeniden yapılanmasını modellemek için seyreltik nitritlerin katılmasından dolayı iletkenlik anti bant geçiş modeli, C-BAC ve seyreltik bismutların katılmasından dolayı da değerlik anti bant geçiş modeli, V-BAC kullanılmıştır.

**Anahtar kelimeler:** Elektronik bant yapısı, gerilme, seyreltik bismutlar, seyreltik nitritler, anti bant geçiş modeli, bant boşluğu enerjisi, spin yörünge etkileşim enerjisi



*I dedicate this work to my family...*



## ACKNOWLEDGEMENTS

Firstly, I would like to express my sincere gratitude to my supervisor Prof. Dr. Beşire GÖNÜL for the continuous support of my M.Sc study and related research, for her patience, motivation, and immense knowledge. Her guidance helped me in all the time of research and writing of this thesis. I could not have imagined having a better advisor and mentor for my M.Sc study.

Besides my co-supervisor Dr. Ömer Lütfi ÜNSAL , I would like to thank the rest of my thesis committee: Prof. Dr. Mustafa ÖZTAŞ and Assoc. Prof. Dr. Vural Emir KAFADAR for their insightful comments and encouragement, but also for the hard question which incited me to widen my research from various perspectives.

## TABLE OF CONTENTS

	Page
ABSTRACT . . . . .	v
ÖZET . . . . .	vi
ACKNOWLEDGEMENTS . . . . .	viii
TABLE OF CONTENTS . . . . .	ix
LIST OF TABLES . . . . .	xi
LIST OF FIGURES . . . . .	xii
LIST OF SYMBOLS . . . . .	xvi
CHAPTER 1 . . . . .	1
INTRODUCTION . . . . .	1
CHAPTER 2 . . . . .	5
THEORETICAL MODELS FOR BAND STRUCTURE . . . . .	5
2.1 Introduction . . . . .	5
2.2 Band Anti-crossing Models . . . . .	8
2.2.1 Conduction Band Anti-crossing Model . . . . .	8
2.2.2 Valence Band Anti-crossing Model . . . . .	10
2.2.3 Valence Band Energy Level . . . . .	12
2.3 Interpolation method (Vegards Law) . . . . .	14
2.4 Strain Theory . . . . .	16
2.5 Summary . . . . .	17
CHAPTER 3 . . . . .	18
CALCULATION OF BAND STRUCTURE OF INDIUM BASED III-V BISMIDES ALLOYS . . . . .	18
3.1 Introduction . . . . .	18

3.2	InAs <sub>0.88</sub> Bi <sub>0.12</sub> . . . . .	19
3.3	InP <sub>0.88</sub> Bi <sub>0.12</sub> . . . . .	24
3.4	InSb <sub>0.88</sub> Bi <sub>0.12</sub> . . . . .	28
3.5	Summary . . . . .	32
<b>CHAPTER 4 . . . . .</b>		<b>33</b>
<b>CALCULATION OF BAND STRUCTURE OF ARSENIDE BASED III-V DILUTE BISMIDES AND NITRIDES . . . . .</b>		<b>33</b>
4.1	Introduction . . . . .	33
4.2	GaAs <sub>0.88</sub> Bi <sub>0.12</sub> . . . . .	33
4.3	GaAs <sub>0.94</sub> N <sub>0.06</sub> . . . . .	37
4.4	GaAs <sub>0.82</sub> N <sub>0.06</sub> Bi <sub>0.12</sub> . . . . .	39
4.5	Summary . . . . .	43
<b>CHAPTER 5 . . . . .</b>		<b>45</b>
THESIS SUMMARY AND FUTURE WORK . . . . .		45
<b>REFERENCES . . . . .</b>		<b>47</b>

## LIST OF TABLES

	<b>Page</b>
<b>Table 2.1</b> The electronegativity and covalent radius values for related elements [18–20]. . . . .	8
<b>Table 2.2</b> The material parameters for Ga based binary materials required in our calculations [26–28]. . . . .	14
<b>Table 2.3</b> The material parameters for In based binary materials required in our calculations [26–28]. . . . .	14
<b>Table 3.1</b> The material parameters for ternary materials [4, 13, 26, 35].	19
<b>Table 3.2</b> The lattice constants used in our calculations for binary materials [26, 39]. . . . .	23

## LIST OF FIGURES

	Page
<b>Figure 2.1</b> Schematic illustration of band structure of a) GaAsN and b) GaAsBi showing CB, HH, LH, SO, nitrogen energy level, $E_N$ and bismuth energy level, $E_{Bi}$ . . . . .	6
<b>Figure 2.2</b> Schematic diagram showing (a)CHCC (b)CHSH and (c)phonon-assisted CHSH Auger recombination processes [11]. . . . .	7
<b>Figure 2.3</b> The BAC effects on the N level and GaAs CB [21]. . . . .	9
<b>Figure 2.4</b> Calculated dispersion of the $E_-$ and $E_+$ subbands in GaAsN at three different pressures [3]. . . . .	10
<b>Figure 2.5</b> (a) The VB of GaAs and the localized Bi level and (b) the variations of $E_+$ and $E_-$ levels as a function of wavefactor for 6% bismuth [5]. . . . .	13
<b>Figure 2.6</b> Schematic diagram (a) tensile-strained and (b) compressively-strained layers grown on thick substrates [30]. . . . .	16
<b>Figure 2.7</b> Schematic diagram showing the bulk band structure of three $\text{In}_{1-x}\text{Ga}_x\text{As}$ ternary strained layers grown on InP substrate [31]. . . . .	17
<b>Figure 3.1</b> Variation of relative energy locations for $E_{HH/LH+}$ and $E_{HH/LH-}$ as a function of Bi concentration for $\text{InAs}_{1-x}\text{Bi}_x$ on InAs. . . . .	20
<b>Figure 3.2</b> Energy locations $E_+$ and $E_-$ of the heavy hole, light hole and split-off bands for $\text{InAs}_{1-x}\text{Bi}_x/\text{InAs}$ as a function of Bi concentration up to 12 %. . . . .	20

<b>Figure 3.3</b>	Variation of $E_g$ and $\Delta_0$ as a function of Bi concentration for $\text{InAs}_{1-x}\text{Bi}_x/\text{InAs}$ . . . . .	21
<b>Figure 3.4</b>	Estimated variation of band edge energy due to Bi (up to 12 %) and N (up to 6 %) incorporation in $\text{InAs}_{1-x-y}\text{N}_y\text{Bi}_x$ on InAs substrates. . . . .	22
<b>Figure 3.5</b>	The strain along the growth x and z direction versus bismuth concentration in the $\text{InAs}_{1-x}\text{Bi}_x/\text{InAs}$ . . . . .	23
<b>Figure 3.6</b>	Estimated variation of strain due to Bi (up to 12 %) and N (up to 6 %) incorporation in $\text{InAs}_{1-x}\text{Bi}_x$ and $\text{InN}_y\text{As}_{1-x-y}\text{Bi}_x$ on InAs substrates. . . . .	23
<b>Figure 3.7</b>	Variation of relative energy locations for $E_{HH/LH+}$ and $E_{HH/LH-}$ as a function of Bi concentration for $\text{InP}_{1-x}\text{Bi}_x$ on InP substrates. . . . .	24
<b>Figure 3.8</b>	Energy locations $E_+$ and $E_-$ of the heavy hole, light hole and split-off bands for $\text{InP}_{1-x}\text{Bi}_x/\text{InP}$ as a function of Bi concentration up to 12 %. . . . .	25
<b>Figure 3.9</b>	Variation of $E_g$ and $\Delta_0$ as a function of Bi concentration for $\text{InP}_{1-x}\text{Bi}_x/\text{InP}$ . . . . .	25
<b>Figure 3.10</b>	Variation of $E_g$ and $\Delta_0$ as a function of Bi concentration for $\text{InP}_{1-x}\text{Bi}_x/\text{InP}$ . . . . .	26
<b>Figure 3.11</b>	Estimated variation of band edge energy due to Bi (up to 12 %) and N (up to 6 %) incorporation in $\text{InP}_{1-x-y}\text{N}_y\text{Bi}_x$ on InP substrates. . . . .	26
<b>Figure 3.12</b>	The strain along the growth x and z direction versus bismuth concentration in $\text{InP}_{1-x}\text{Bi}_x/\text{InP}$ . . . . .	27
<b>Figure 3.13</b>	Estimated variation of strain due to Bi (up to 12 %) and N (up to 6 %) incorporation in $\text{InP}_{1-x}\text{Bi}_x$ and $\text{InN}_y\text{P}_{1-x-y}\text{Bi}_x$ on InP substrates. . . . .	28

<b>Figure 3.14</b>	Variation of relative energy locations for $E_{HH/LH+}$ and $E_{HH/LH-}$ as a function of Bi concentration for $\text{InSb}_{1-x}\text{Bi}_x$ on InSb substrates. . . . .	29
<b>Figure 3.15</b>	Variation of $E_g$ and $\Delta_0$ as a function of Bi concentration for $\text{InSb}_{1-x}\text{Bi}_x/\text{InSb}$ . . . . .	29
<b>Figure 3.16</b>	Energy locations $E_+$ and $E_-$ of the heavy hole, light hole and split-off bands for $\text{InSb}_{1-x}\text{Bi}_x/\text{InSb}$ as a function of Bi concentration up to 12 %. . . . .	30
<b>Figure 3.17</b>	The strain along the growth x and z direction versus bismuth concentration in the $\text{InSb}_{1-x}\text{Bi}_x/\text{InSb}$ . . . . .	31
<b>Figure 3.18</b>	Estimated variation of strain due to Bi (up to 12 %) and N (up to 6 %) incorporation in $\text{InSb}_{1-x}\text{Bi}_x/\text{InSb}$ and $\text{InN}_y\text{Sb}_{1-x-y}\text{Bi}_x$ on InSb substrates. . . . .	31
<b>Figure 4.1</b>	Variation of relative energy positions for $E_{HH/LH+}$ and $E_{HH/LH-}$ as a function of Bi concentration for $\text{GaAs}_{1-y}\text{Bi}_y$ on GaAs substrates. . . . .	34
<b>Figure 4.2</b>	Energy locations $E_+$ and $E_-$ of the heavy hole, light hole and split-off bands for $\text{GaAs}_{1-y}\text{Bi}_y/\text{GaAs}$ as a function of Bi concentration up to 12 %. . . . .	35
<b>Figure 4.3</b>	Variation of $E_g$ and $\Delta_0$ as a function of Bi concentration for $\text{GaAs}_{1-y}\text{Bi}_y/\text{GaAs}$ . . . . .	36
<b>Figure 4.4</b>	The strain along the growth direction versus bismuth concentration in the $\text{GaAs}_{1-y}\text{Bi}_y/\text{GaAs}$ . . . . .	37
<b>Figure 4.5</b>	Variation of relative energy positions for $E_+$ and $E_-$ as a function of Bi concentration for $\text{GaAs}_{1-x}\text{N}_x/\text{GaAs}$ . . . . .	38
<b>Figure 4.6</b>	The strain along the growth direction versus nitrogen concentration in the $\text{GaAs}_{1-x}\text{N}_x/\text{GaAs}$ . . . . .	39

<b>Figure 4.7</b>	Variation of both $E_+$ and $E_-$ levels as a function of Bi (12%) and N (6%) concentration for $\text{GaAs}_{1-y}\text{Bi}_y/\text{GaAs}$ and $\text{GaAs}_{1-x}\text{N}_x/\text{GaAs}$ . . . . .	40
<b>Figure 4.8</b>	Energy locations $E_+$ and $E_-$ of conduction band, heavy hole, light hole and split-off bands for $\text{GaAs}_{1-x-y}\text{N}_x\text{Bi}_y/\text{GaAs}$ as a function of Bi (12%) and N (6%) concentration. . . . .	41
<b>Figure 4.9</b>	Variation of $E_g$ and $\Delta_0$ as a function of Bi (12%) and N (6%) concentration for $\text{GaAs}_{1-x-y}\text{N}_x\text{Bi}_y/\text{GaAs}$ . . . . .	42
<b>Figure 4.10</b>	Estimated variation of band edge energy and wavelenght due to Bi (up to 12 %) and N(up to 6 %) incorporation in $\text{GaAs}_{1-x-y}\text{N}_x\text{Bi}_y/\text{GaAs}$ . . . . .	42
<b>Figure 4.11</b>	Estimated variation of strain due to Bi (up to 12 %) and N (up to 6 %) incorporation in $\text{GaAs}_{1-x}\text{N}_x/\text{GaAs}$ and $\text{GaAs}_{1-y}\text{Bi}_y/\text{GaAs}$ . . . . .	43



## LIST OF SYMBOLS

$\hbar$  : Planck's constant

$k_B$  : Boltzmann's constant

$E_g$  : Band gap(eV)

$\Delta_0$  : Spin-orbit splitting(eV)

$C_{11}$  : Elastic Stiffness constant

$C_{12}$  : Elastic Stiffness constant

$C_{44}$  : Elastic Stiffness constant

$b$  : Deformation potential(eV)

$a_0$  : Lattice constant Å

$m_e^*$  : Electron effective mass

$a_c$  : Hydrostatic deformation potential for conduction band

$a_v$  : Hydrostatic deformation potential for valence band

$\gamma_1$  : Luttinger parameter

$\gamma_2$  : Luttinger parameter

$\gamma_3$  : Luttinger parameter

$\Delta E_{CBM}$  : Conduction band maximum

$\Delta E_{VBM}$  : Valence band maximum

$E_{Bi-so}$  : The location of corresponding spin-orbit split-off level

$\Delta E_{SO}$  : The spin-orbit split-off band offset

$E_{Bi}$  : Energy of the localized Bi level

$E_N$  : Energy of the localized N level

$C_{Bi}$  : Coupling parameter

## CHAPTER 1

### INTRODUCTION

Compound semiconductors offer a possibility to get semiconductor materials with a variety of wavelengths having a direct band gap material which is essential to get an efficient light emission in light emitting diodes (LED) and lasers. III-V compound semiconductors have especially preferred in diode lasers to have an emission wavelength at 1.3 and 1.55  $\mu\text{m}$ . This wavelength range is quite important in telecommunication since dispersion is zero and the losses are minimum at these stated wavelengths. After the invention of semiconductor lasers in 1960s [1] semiconductor diode lasers have been widely and successfully used in laser printing, optical data storing, as a pump mechanism for solid state lasers, and in information and telecommunication technologies. The widely used area of III-V compound semiconductor materials shows that III-V compound semiconductors play an important role for electronic and optoelectronic device applications in modern technology.

Lasers which emit light in the wavelength range of 1.3 and 1.55  $\mu\text{m}$  require semiconductor materials with a direct bandgap range between 0.95 and 0.8 eV. Semiconductor laser diodes are forward biased pn junction devices. The pn junction must be grown on a suitable substrate material. Unfortunately the number of available good quality and cheap binary substrates were limited. The only selections were GaAs and InP in earlier investigations. In order to have a uniform growth of layers on top of each other, there is a requirement of lattice-matching of which the lattice constant of alloy semiconductor must be so close to the lattice constant of substrate materials. At that time, scientists couldn't find a suitable alloy semiconductor which is lattice matched to GaAs substrate in the long wavelength range. Thus InGaAsP and InGaAlAs on InP substrates has been considered as a material system which emits light being greater than 1.1  $\mu\text{m}$ . These quaternary materials are still widely used as a laser material in long wavelength telecommunications. However, the performance of these InP based semiconductor lasers operating at long wavelengths has several disadvantages.

The performance of these lasers are limited due to high threshold currents and temperature instability. A great deal of scientific and engineering research has been given to reveal the reasons for high threshold current and temperature instability and then it is stated that loss mechanisms of Auger recombination and intervalence band absorption are the most important reason for these behaviours. In addition, both loss mechanisms and threshold current increase with increasing temperature. Therefore, an intense effort to reach an alternative solution to InP epitaxy has been paid and new exotic compound semiconductor materials have been searched. The exotic new materials has been expected to satisfy the following requirements; First of all, electrons should be confined in deeper quantum wells due to prevent the leakage into the barrier because of lighter mass of electrons. Secondly, photons must be confined in gain region which is only possible by means of the increase in refractive index difference between layers and substrate material. Finally, in order to eliminate the important loss mechanisms of Auger recombination and intervalence band absorption, an alloy with a  $\Delta_0$  being greater than the forbidden  $E_g$  is required. In order to satisfy all these requirements, it is necessary to engineer the band gap, band alignment and tune the lattice matching between layers and substrate, i.e. strain. It should be notice that a lattice-match growth is preferable to get high quality and reliable devices on suitable substrates.

Due to limitations of the well known long wavelength laser materials of InGaAsP and InGaAlAs on InP substrates has been pushed the people to look for an alternative gain material that can be grown on GaAs substrate. Diode lasers constructed from new material systems such as dilute nitrides and bismides can be considered as promising candidates to eliminate high threshold current and temperature instability. Carrier confinement can be improved due to ideal band alignments of alloys on GaAs substrates. Optical confinement can also be improved due to the larger refractive index difference between GaAs and AlGaAs compared to that between InP and the quaternary alloys. Layers can be grown on top of each other uniformly as lattice-match and lattice-mismatch with reasonable thicknesses. This brings a great advantage and flexibility to choose a proper material with an ideal band structure and material with the required bandgap. Furthermore the epitaxial growth can be achieved on larger GaAs substrates since GaAs is a more intense material compared to InP material allowing easy monolithic growth on GaAs.

An alternative active material, GaInNAs, that can be grown on GaAs is proposed by Kondow et al [2]. This new material system called as dilute nitrides was very interesting due to their unusual physical properties compared to that of

the conventional III-V counterparts. According to the general rules of the III-V semiconductors, a decrease in lattice constant increases the bandgap. Nitrogen, N, atom with a large electronegativity and a small covalent radius have a strong negative bowing parameter. Thus when N is introduced to GaAs its bandgap decreases sharply contrary to the conventional semiconductors. This unusual band structure allows to the fabrication of long wavelength lasers.

Bismuth, Bi, containing III-V semiconductor alloys can be considered as another alternative active material grown on GaAs substrates. The incorporation of small amounts of Bi into GaAs leads attractive properties such as a strong decrease in  $E_g$  and an increase in  $\Delta_0$  which was one of the requirement to remove loss mechanisms of IVBA and Auger recombination. Thus, these alloys having the desired band structure has been considered as a light emitting device in near infrared. These alloys are named as dilute bismides.

Dilute bismide and nitrides have some similar and dissimilar properties. In both dilute nitrides and bismides, there is a reduction in bandgap due to introduced isovalent-impurity atom. In dilute nitrides, the incorporation of N into GaAs produce a resonant defect level above the conduction band edge, CBE, of GaAs. The reduction in bandgap energy of dilute nitrides is due to the interaction of the N related impurity state with the conduction band of the host III-V semiconductor binary alloys. Walukiewicz et al [3] introduced a successful theory which takes into account the band anticrossing interaction between localized N-related states and the CBE of the host binary alloy. This model is named as conduction band anti-crossing model, C-BAC, that cause a splitting of CB into two different states. On the other hand, the incorporation of Bi into GaAs produce a resonant defect level close to the valence band edge, VBE, of the binary host material. The reduction in bandgap energy of dilute bismides is due to the interaction of the Bi impurity state with the valence band, i.e. the heavy hole, HH, and light hole, LH bands of the host III-V semiconductor binary alloys. These variations in band structure can be described by valence band anti-crossing model, V-BAC [4, 5]. The interaction of Bi impurity state with the spin orbit split off band of the host enhances the spin orbit splitting in III-V bismides allowing to reduce the loss mechanisms which is a great benefit. These unusual and interesting properties have been pushed the people to incorporate small amounts of nitrogen and bismide simultaneously in the same alloy resulting dilute bismide and nitride alloys of GaAsBiN.

This study provides a detailed investigation of the reconstruction of the conduction band edge with incorporation of N into III-V binaries by means of using

C-BAC model and reconstruction of valence band edge with incorporation of Bi into III-V binaries by means of using V-BAC model.

Information about the theoretical part of the thesis was given in chapter 2.

In chapter 3, we have presented an analysis of electronic band structure and strain values of ternary  $\text{InAs}_{1-x}\text{Bi}_x$ ,  $\text{InP}_{1-x}\text{Bi}_x$  and  $\text{InSb}_{1-x}\text{Bi}_x$  materials on GaAs substrates.

Chapter 4 presents the calculated results of the electronic band structures and strain values of ternary  $\text{GaAs}_{1-x}\text{N}_x$  and  $\text{GaAs}_{1-y}\text{Bi}_y$  and the quaternary  $\text{GaAs}_{1-x-y}\text{N}_x\text{Bi}_y$  on GaAs substrates.

Chapter 5 covers the thesis summary and future work.



## CHAPTER 2

### THEORETICAL MODELS FOR BAND STRUCTURE

#### 2.1 Introduction

III-V compound semiconductor materials play an important role for device applications of electronics and optoelectronics devices in modern technology. Incorporation of a small concentration of Bi and N atoms into a conventional III-V semiconductor host materials produces dilute bismide and nitride alloys. During the past decade, III-V dilute nitride and bismide alloys have attracted a great deal of attention due to their both unique physical and technical properties as well as their potential for specific optoelectronic device applications. The replacement of a small concentration of arsenides, antimonides or phosphides by bismuth or nitrogen in III-V host material produces a large band gap reduction,  $E_g$ . Thus the band gap of the resulting dilute III-V-N and Bi alloys can be adjusted to specific energies for optoelectronic devices by changing the nitrogen or bismuth concentration. Bismuth concentration also produces a large bowing in  $\Delta_0$  of the host material. The changes both in  $E_g$  and  $\Delta_0$  has been explained using a valence band anti-crossing, V-BAC, for dilute bismides. This is due to the interaction between the bismuth energy level and the host GaAs. The conduction band anti-crossing, C-BAC, describes the rapid reduction in bandgap for dilute nitride alloys [6]. As a result of band anti-crossing, BAC, models, valence band and conduction band split into two characteristic subbands  $E_+$  and  $E_-$  and also, valence band splits the heavy hole, light hole and split-off bands into a series of  $E_+$  and  $E_-$  subbands energy level.

When a small concentration of bismuth and nitrogen are incorporated into a III-V semiconductor host material, Bi and N related impurity energy levels lies inside the valence band and the conduction band edge of the host material, respectively. Thus, bismuth primarily affects the VB, while nitrogen affects the CB [7]. Figure 2.1 shows the schematic diagram of band structures of dilute  $\text{GaAs}_{1-x}\text{N}_y$  and  $\text{GaAs}_{1-y}\text{Bi}_y$ .

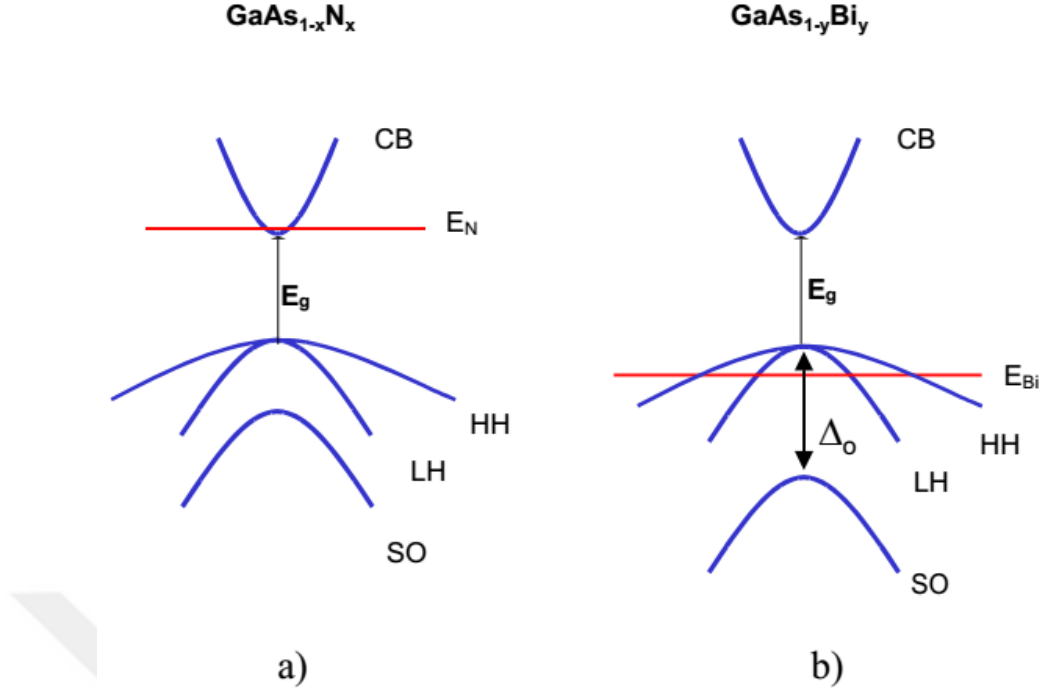


**Figure 2.1** Schematic illustration of band structure of a) GaAsN and b) GaAsBi showing CB, HH, LH, SO, nitrogen energy level,  $E_N$  and bismuth energy level,  $E_{Bi}$ .

The band gap reduction,  $E_g$  in both dilute nitrides and bismides and strong spin-orbit splitting energy,  $\Delta_0$  in dilute bismide alloys are believed to be due to the interaction of the nitrogen energy level,  $E_N$  and bismuth,  $E_{Bi}$  with the host band edges. Moreover, bismuth containing III-V alloys offer the possibility to suppress Auger recombination [8]. Auger recombination and IVBA decreases the efficiency of semiconductor lasers in the near- and mid-infra-red (mid-IR) region of spectrum [9]. To suppress or eliminate these loss mechanism one needs to achieve a  $\Delta_0$  bigger than the  $E_g$  energy. The situation of  $\Delta_0 > E_g$  prohibits Auger recombination and IVBA transitions, because energy and momentum can no longer be conserved [10]. Therefore, dilute bismide plays a significant role to reduce band gap energy,  $E_g$  and increase spin-orbit splitting energy,  $\Delta_0$ .

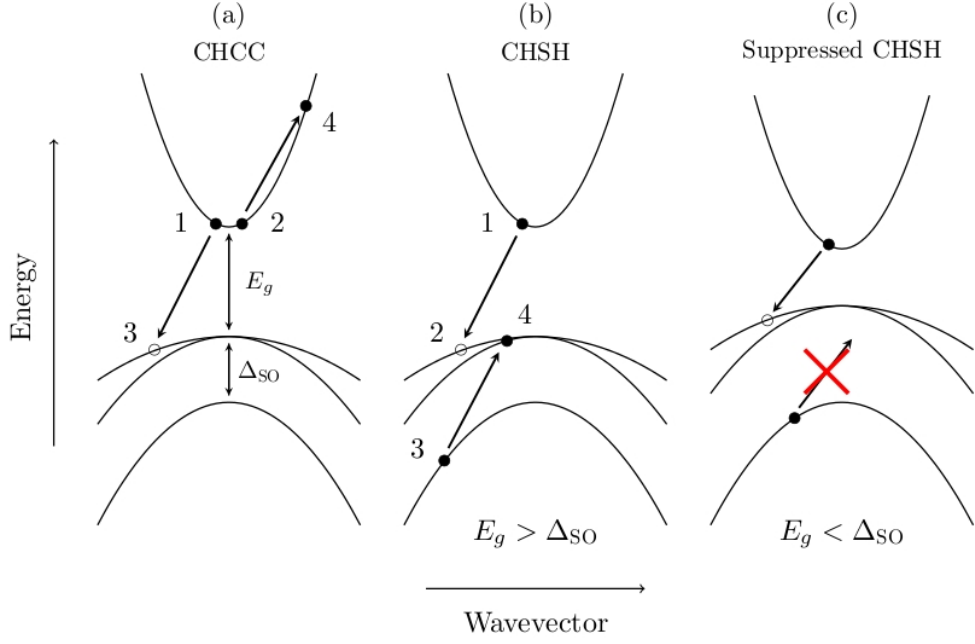


**Figure 2.2** Schematic diagram showing (a)CHCC (b)CHSH and (c)phonon-assisted CHSH Auger recombination processes [11].

Figure 2.2 (a) illustrates the CHCC Auger recombination in which an electron in a CB (1) recombines with a hole in a VB (3) with the delivered energy stimulating a second electron in the CB (2) to an empty higher conduction state (4). After all these steps energy and momentum are conserved. In a CHSH Auger recombination in which an electron in a CB (1) recombines with a hole in a VB (2) with the delivered energy stimulating a hole in the VB (4) to the spin split off band (3). Again energy and momentum are conserved. When the spin-orbit splitting band energy,  $\Delta_0$  is greater than the band gap energy,  $E_g$ , CHSH process, is forbidden due to conservation of energy. Since there is no available energy state to excite a hole to the spin split off band [11].

The aim of this chapter is to give information about the theoretical part of this thesis. For this purpose, we present the C-BAC for dilute nitrides and V-BAC for dilute bismides. Secondly, we provide the interpolation method to calculate the necessary band parameters. Finally, we present the theory of strain to calculate strain values of ternary and quaternary III-V bismide and nitride alloys.



## 2.2 Band Anti-crossing Models

III-V conventional semiconductor materials have the tendency of increasing  $E_g$  with decreasing lattice constant. On the other hand, dilute bismide and dilute III-V-N alloys have large reductions in fundamental  $E_g$  with a decrease in lattice constant. According to Shan et al [12] have demonstrate that this uncommon behaviour can be accepted within a simple BAC for dilute nitrides. The band anti-crossing model is based on the interaction of the CB energy level with the localized N related energy level  $E_N$ . Alberi et al [13] proposed a similar BAC model that describes the splittings in VB for dilute bismides. Both models illustrate how we can reconstruct the CB and VB as a result of the interaction of the respective bands with nitrogen impurity level,  $E_N$ , and bismuth impurity level,  $E_{Bi}$ .

### 2.2.1 Conduction Band Anti-crossing Model

When As atom in binary GaAs is replaced by an isovalent impurity N, a resonant defect level lying above the CB edge of GaAs arises [14, 15]. This defect level is due to the large difference in electronegativity and atomic size between N and As [16, 17]. The radii and electronegativity values of usually used elements are shown in Table 2.1.

**Table 2.1** The electronegativity and covalent radius values for related elements [18–20].

Element	Electronegativity	Covalent radius(Å)
Si	1.90	1.17
Ga	1.81	1.25
P	2.19	1.1
N	3.05	0.7
As	2.18	1.21

The C-BAC model explains the interaction of the localized defect states with the CBE for a two-level system. As a result of this interaction there is a splitting of the CB into two characteristic subbands that are typically labeled  $E_+$  and  $E_-$  for the high and low energy bands respectively. Figure 2.3 clearly shows that binary GaAs conduction band energy level interaction with defect nitrogen energy levels and this interaction cause the conduction band to split into two subbands  $E_+$  and  $E_-$ . Figure 2.3 also illustrates the increase in splitting as a function of N

concentration.

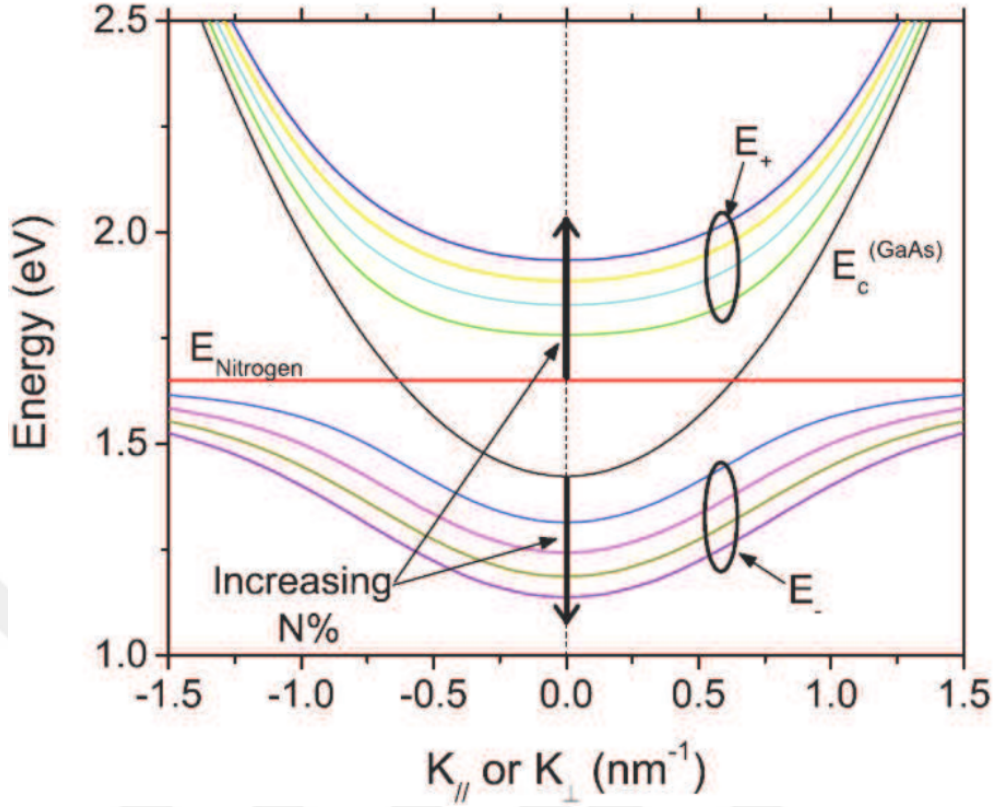


**Figure 2.3** The BAC effects on the N level and GaAs CB [21].

In order to understand the conduction band anti-crossing model, one needs to consider, a simple band model with interacting localized nitrogen energy level and conduction band edge level. Shan et al [12] proposed the following standard procedures and assumed that the interaction of the two types of states can be treated as a perturbation which leads to the following eigenvalue problem of

$$\begin{vmatrix} E - E_M & V_{MN} \\ V_{MN} & E - E_N \end{vmatrix} = 0 \quad (2.1)$$

where  $E_M$  and  $E_N$  are the extended state in the CB of the host GaAs matrix and the energy level of the N localized level.  $V_{MN}$  refers to interaction between localized N level and CBE level and is given [22] by

$$V_{MN} = C_{MN}\sqrt{x} \quad (2.2)$$

where  $C_{MN}$  is the coupling constant and  $x$  is the N composition in the III-V nitride alloys. The solution to the eigenvalue problem in Equation 2.1 is then

$$E_{\pm} = \frac{E_N + E_M \pm \sqrt{(E_N - E_M)^2 + 4xC_{MN}^2}}{2} \quad (2.3)$$

Equation 2.3 shows that the conduction band energy level of the host GaAs binary material splits into two subbands  $E_+$  and  $E_-$ . Figure 2.4 shows the results of calculations of  $E_+$  and  $E_-$  at three different values of hydrostatic pressure.

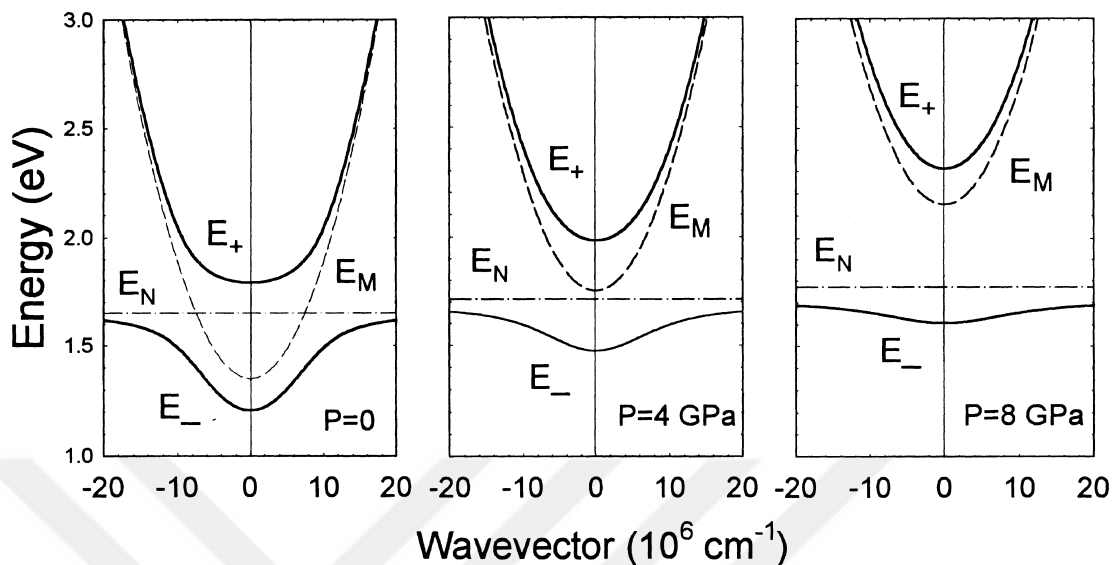


**Figure 2.4** Calculated dispersion of the  $E_-$  and  $E_+$  subbands in GaAsN at three different pressures [3].

### 2.2.2 Valence Band Anti-crossing Model

When Bi atom is incorporated into the binary III-V semiconductor alloys, localized bismuth energy level lie near the VBE of the host semiconductor material. This localized energy level, then interact with the extended states of the host binary semiconductor material. The interaction leads a reconstruction of the VB of the heavy hole, light hole and split-off bands to split into a series of  $E_+$  and  $E_-$  subbands energy level. In this subsection, we explain to k.p formalism which was used earlier [23] to describe the rearrangement of VB in the bismuth containing III-V semiconductor materials. The interaction of the bismuth energy level with the VB of the corresponding host binary semiconductor material was described by a  $12 \times 12$  Hamiltonian which includes, 6 p-like VB states of the host semiconductor material and the 6 localized p-like states of the incorporated Bi impurity atoms [24]. The resultant solution to the Hamiltonian produces six doubly degenerate eigenvalues that characterize three pairs of spin-degenerate subbands formed by  $E_{LH\pm}$ ,  $E_{HH\pm}$  and  $E_{SO\pm}$  due to the hybridization effects between the VB and Bi impurity states [25]. At the point, where  $k$  is different from zero, the  $12 \times 12$  matrix can be written as:

$$\begin{pmatrix}
H & \alpha & \beta & 0 & \frac{i\alpha}{\sqrt{2}} & -\sqrt{2}i\beta & Vx & 0 & 0 & 0 & 0 & 0 \\
\alpha^* & L & 0 & \beta & \frac{iD}{\sqrt{2}} & \sqrt{\frac{3}{2}}i\alpha & 0 & Vx & 0 & 0 & 0 & 0 \\
\beta^* & 0 & L & -\alpha & -\sqrt{\frac{3}{2}}i\alpha & \frac{iD}{\sqrt{2}} & 0 & 0 & Vx & 0 & 0 & 0 \\
0 & \beta^* & -\alpha^* & H & -\sqrt{2}i\beta & -\frac{i\alpha^*}{\sqrt{2}} & 0 & 0 & 0 & Vx & 0 & 0 \\
\frac{i\alpha^*}{\sqrt{2}} & -\frac{iD}{\sqrt{2}} & \sqrt{\frac{3}{2}}i\alpha & \sqrt{2}i\beta & S & 0 & 0 & 0 & 0 & 0 & Vx & 0 \\
\sqrt{2}i\beta^* & -\sqrt{\frac{3}{2}}i\alpha^* & -\frac{iD}{\sqrt{2}} & \frac{i\alpha}{\sqrt{2}} & 0 & S & 0 & 0 & 0 & 0 & 0 & Vx \\
Vx & 0 & 0 & 0 & 0 & 0 & E_{Bi} & 0 & 0 & 0 & 0 & 0 \\
0 & Vx & 0 & 0 & 0 & 0 & 0 & E_{Bi} & 0 & 0 & 0 & 0 \\
0 & 0 & Vx & 0 & 0 & 0 & 0 & 0 & E_{Bi} & 0 & 0 & 0 \\
0 & 0 & 0 & Vx & 0 & 0 & 0 & 0 & 0 & E_{Bi} & 0 & 0 \\
0 & 0 & 0 & 0 & Vx & 0 & 0 & 0 & 0 & 0 & E_{Bi-SO} & 0 \\
0 & 0 & 0 & 0 & 0 & Vx & 0 & 0 & 0 & 0 & 0 & E_{Bi-SO}
\end{pmatrix} \quad (2.4)$$

where

$$H = -\frac{\hbar^2}{2m_o} [(k_x^2 + k_y^2) (\gamma_1 + \gamma_2) + k_z^2 (\gamma_1 - 2\gamma_2)] \quad (2.5a)$$

$$L = -\frac{\hbar^2}{2m_o} [(k_x^2 + k_y^2) (\gamma_1 - \gamma_2) + k_z^2 (\gamma_1 + 2\gamma_2)] \quad (2.5b)$$

$$\alpha = \sqrt{3} \frac{\hbar^2}{m_o} [k_x (k_x - ik_y) \gamma_3] \quad (2.5c)$$

$$\beta = \frac{\sqrt{3}}{2} \frac{\hbar^2}{m_o} [(k_x^2 - k_y^2) \gamma_2 - 2ik_x k_y \gamma_3] \quad (2.5d)$$

$$D = L - H \quad (2.5e)$$

$$S = \frac{1}{2} (L + H) - \Delta_0 \quad (2.5f)$$

At the  $\Gamma$  point, where  $k = 0$ , all the off-diagonal elements of the 6 x 6 portion of the Hamiltonian matrix becomes zero. Then, the solution of the Hamiltonian matrix produces four different eigenvalues similar to the  $E_+$  and  $E_-$  subbands of the heavy hole, light hole and split-off bands. The solutions of the Hamiltonian for  $k = 0$  are given by following equations of [4].

$$E_{LH/HH\pm} = \frac{1}{2} \left( H + E_{Bi} \pm \sqrt{H^2 - 2HE_{Bi} + E_{Bi}^2 + 4V^2} \right) \quad (2.6)$$

$$E_{SO\pm} = \frac{1}{2} \left( S + E_{Bi-SO} \pm \sqrt{S^2 - 2SE_{Bi-SO} + E_{Bi-SO}^2 + 4V^2} \right) \quad (2.7)$$

with

$$H = L = \Delta E_{VBM}x \quad (2.8a)$$

$$S = \Delta E_{VBM}x - \Delta_0 - \Delta E_{SO}x \quad (2.8b)$$

$$V = C_{Bi}\sqrt{y} \quad (2.8c)$$

where  $\Delta E_{VBM}$  and  $\Delta E_{SO}$  in the above statement indicate the difference in the  $E_{VBM}$  and the  $E_{SO}$ .  $\Delta_0$  is the spin orbit splitting energy,  $V$  refers to interaction

between localized bismuth level and VBE level and  $C_{Bi}$  is the coupling constant.  $E_{Bi}$  and  $E_{Bi-SO}$  are the Bi related impurity levels corresponding to the heavy hole, light hole and split-off bands [25].

In addition, the  $E_g$  reduction calculated from the virtual crystal approximation, VCA, and can be written as [23],

$$E_{CB} = E_g - \Delta E_{CBM}x \quad (2.9)$$

where  $E_g$  refers the bandgap energy of the corresponding binary host material and  $\Delta E_{CBM}$  is its CB offset.

### 2.2.3 Valence Band Energy Level

According to Alberi et al's V-BAC model [13], the energies of the  $E_+$  and  $E_-$  levels are given by

$$E_{\pm}(AB_{1-x}Bi_x) = \frac{E_{V,AB} + E_{Bi} \pm \sqrt{(E_{V,AB} - E_{Bi})^2 + 4V_{MBi}^2}}{2} \quad (2.10)$$

where  $E_{V,AB}$  is the energy of VBM of binary AB host material,  $E_{Bi}$  is the energy of the Bi level lying below the VBM of AB.  $C_{Bi}$  is the coupling parameter between the Bi level and AB host.  $V_{MBi}$  is the matrix element describing the interaction between localized bismuth level and valence band edge level.

$$V_{MBi} = C_{Bi}\sqrt{x} \quad (2.11)$$

where  $C_{Bi}$  is the coupling constant and  $x$  is the Bi composition in the III-V-Bi alloys.

Since Bi impurity energy level lies below the VBM of AB and interaction between Bi level and AB VBM, valence band maximum in AB moves an upward direction and this leads a band gap reducton,  $E_g$ . Figure 2.5 shows the interaction between localized Bi level and VB energy level of GaAs. As can be seen from figure 2.5 VB energy level splits into two sub-bands,  $E_+$  and  $E_-$ .

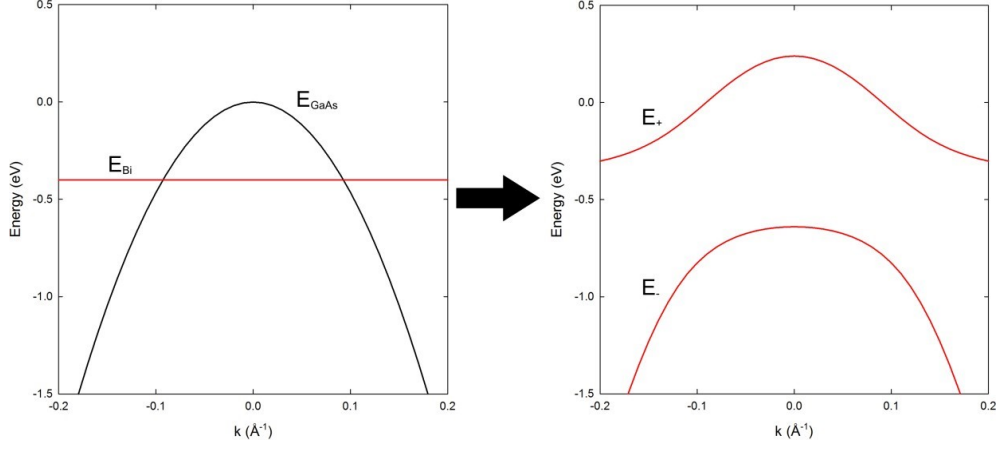


**Figure 2.5** (a) The VB of GaAs and the localized Bi level and (b) the variations of  $E_+$  and  $E_-$  levels as a function of wavefactor for 6% bismuth [5].

The conduction band energy level is uninfluenced in valence band anti-crossing model since the Bi energy level is located at much lower energy than the CB. Thus the  $E_g$  of  $AB_{1-x}Bi_x$  is given by,

$$E_{g,AB_{1-x}Bi_x} = E_{C,AB} - E_{+,ABBi} \quad (2.12)$$

which can be simplified to

$$E_{g,AB_{1-x}Bi_x} = E_{g,AB} - \Delta E_{VBAC} \quad (2.13)$$

where  $\Delta E_{VBAC}$  refers to the band  $E_g$  due to Bi incorporation. The VB of  $AB_{1-x}Bi_x$  is described by,

$$E_{\pm}(AB_{1-x}Bi_x) = \frac{E_{V,AB} + E_{Bi} \pm \sqrt{(E_{V,AB} - E_{Bi})^2 + 4V_{MBi}^2}}{2} \quad (2.14)$$

Assuming that the CB edge is constant, the  $E_g$  of  $AB_{1-x}Bi_x$  is

$$E_{g,AB_{1-x}Bi_x} = E_{C,AB} - E_{+,AB_{1-x}Bi_x} \quad (2.15)$$

where  $E_C$  is the CB minimum of AB. Since,

$$E_{Bi} = E_{V,AB} - \Delta E_{VBM-Bi} \quad (2.16)$$

and

$$E_{g,AB} = E_{C,AB} - E_{V,AB} \quad (2.17)$$

where  $\Delta E_{VBM-Bi}$  is the energy difference between the VBM of AB and the Bi level. Using equations 2.14 to 2.17, the  $E_g$  of  $AB_{1-x}Bi_x$  can be simplified to

$$E_{g,AB_{1-x}Bi_x} = E_{g,AB} - \Delta E_{VBAC} \quad (2.18)$$

Here,  $\Delta E_{VBAC}$  refers to the  $E_g$  reduction due to bismuth incorporation, and is given by,

$$\Delta E_{VBAC} = \frac{\Delta E_{VBM-Bi}}{2} \left( \sqrt{1 + \frac{4V_{MBi}^2}{(\Delta E_{VBM-Bi})^2}} - 1 \right) \quad (2.19)$$

The necessary material parameters are given in the Table 2.2-2.3.

**Table 2.2** The material parameters for Ga based binary materials required in our calculations [26–28].

<b>Material</b>	<b>GaAs</b>	<b>GaN</b>	<b>GaBi</b>
Lattice Constant $a_0$ (Å)	5.6532	4.5	6.324
Energy gap $E_o$ (eV)	1.424	3.299	-1.45
Spin-orbit Splitting $\Delta_0$ (eV)	0.341	0.017	2.2
Hydrostatic deformation potential for CB $a_c$ (eV)	-7.17	-2.2	-7.17
Hydrostatic deformation potential for VB $a_v$ (eV)	-1.16	-5.2	-1.16
Elastic Stiffness Constant $C_{11}$ (GPa)	1221.0	293.0	1221.0
Elastic Stiffness Constant $C_{12}$ (GPa)	566.0	159.0	566.0
Elastic Stiffness Constant $C_{44}$ (GPa)	600.0	155.0	600.0
Deformation Potential $b$ (eV)	-2.0	-2.2	-1.6

**Table 2.3** The material parameters for In based binary materials required in our calculations [26–28].

<b>Material</b>	<b>InAs</b>	<b>InSb</b>	<b>InP</b>
Lattice Constant $a_0$ (Å)	6.0583	6.4794	5.8697
Energy gap $E_o$ (eV)	0.417	0.235	1.4236
Spin-orbit Splitting $\Delta_0$ (eV)	0.39	0.81	0.108
Hydrostatic deformation potential for CB $a_c$ (eV)	-5.08	-6.94	-6.00
Hydrostatic deformation potential for VB $a_v$ (eV)	-1.00	-0.36	-0.6
Elastic Stiffness Constant $C_{11}$	832.9	684.7	1011.0
Elastic Stiffness Constant $C_{12}$	452.6	373.5	561.0
Elastic Stiffness Constant $C_{44}$	395.9	311.1	456.0
Deformation Potential $b$ (eV)	-1.8	-2.0	-2.0

### 2.3 Interpolation method (Vegards Law)

In theoretical models of band structure calculations, material parameters such as the bandgap and the lattice constant have an important role. To calculate the

lattice constants and the band gaps as well as effective masses, elastic stiffness constants, we use the linear interpolation (Vegards Law) method [29] by means of the experimentally determined values of the binary compound alloys of ternary and quaternary materials.

The bandgap and the lattice constant of alloys are strongly composition dependent and usually they have a linear relationship. Thus, this linear change can be expressed by Vegard's law [29] taking into account the parameters of the constituent semiconductor materials.

The interpolation method can be used to calculate material parameters for ternary alloys,

$$T_{(ABC)}(x) = xB_{(AC)} + (1 - x)B_{(BC)} \quad (2.20)$$

where  $T_{(ABC)}$  refers to ternary parameters and B is the binary parameters. Equation 2.20 can be written taking into account bowing parameter, C as:

$$T_{(ABC)}(x) = xB_{(AC)} + (1 - x)B_{(BC)} + Cx(1 - x) \quad (2.21)$$

The quaternary material  $A_{1-x}B_xC_yD_{1-y}$  is estimated to be consisted of four binaries: AC, AD, BC, and BD. If one uses a linear interpolation method, the quaternary parameter, Q, can be derived from the binary parameters by

$$Q_{(x,y)} = (1 - x)yB_{(AC)} + (1 - x)(1 - y)B_{(AD)} + xyB_{(BC)} + x(1 - y)B_{(BD)} \quad (2.22)$$

If one of the four binary parameters is missing (e.g., BAD), the quaternary parameter can be close from:

$$Q_{(x,y)} = (1 - x)B_{(AC)} + (x + y - 1)B_{(BC)} + (1 - y)B_{(BD)} \quad (2.23)$$

The quaternary  $A_{1-x}B_xC_yD_{1-y}$  is estimated to be consisted of three binaries: AD, BD, and CD. The associated linear interpolation can be given by

$$Q_{(x,y)} = xB_{(AD)} + yB_{(BD)} + (1 - x - y)B_{(CD)} \quad (2.24)$$

If correlations for the ternary parameters (Ts) are present, the quaternary parameter can be expressed either as  $A_{1-x}B_xC_yD_{1-y}$  or  $A_xB_yC_{1-x-y}D$ .

For  $A_{1-x}B_xC_yD_{1-y}$  alloys:

$$Q_{A_{1-x}B_xC_yD_{1-y}}(x, y) = \frac{x(1-x)[yT_{ABC}(x) + (1-y)T_{ABD}(x)] + y(1-y)[xT_{ACD}(y) + (1-x)T_{BCD}(y)]}{x(1-x) + y(1-y)} \quad (2.25)$$

For  $A_xB_yC_{1-x-y}D$  alloys:

$$Q_{A_xB_yC_{1-x-y}D}(x, y) = \frac{xyT_{ABD}(u) + y(1-x-y)T_{BCD}(v) + x(1-x-y)T_{ACD}(\omega)}{xy + y(1-x-y) + x(1-x-y)} \quad (2.26)$$

where  $u = (1 - x - y)/2$ ,  $v = (2 - x - 2y)/2$  and  $\omega = (2 - 2x - y)/2$ .



## 2.4 Strain Theory

Strain is an important parameter affecting the quality of growth and performance of devices. In heterojunctions system, the lattice constants of the grown materials on top of each other is different in general. This means that the lattice constant of first material does not match exactly to that of the second material. Figure 2.6 shows the schematic diagram of the growth of an epilayer on a substrate material. Figure 2.6(a) illustrates the growth of epilayer with a smaller lattice constant than that of substrate which is called as a tensile strain. Strain will have a positive value in this case. On the other hand, figure 2.6(b) illustrates the growth of an epilayer with a greater lattice constant than that of substrate. This is called as compressive strain and strain will be negative in this situation. Let us consider the growth of an epilayer with a lattice constant  $a_e$  on a substrate with a lattice constant  $a_s$ . The in plane strain along x and y directions is defined by

$$\varepsilon_{\parallel} = \frac{a_s - a_e}{a_e} \quad (2.27)$$

The strain along the growth z-direction is defined by

$$\varepsilon_{\perp} = -\left(\frac{2C_{12}}{C_{11}}\right)\varepsilon_{\parallel} \quad (2.28)$$

where  $C_{11}$  and  $C_{12}$  are the elastic stiffness constants of semiconductor material.

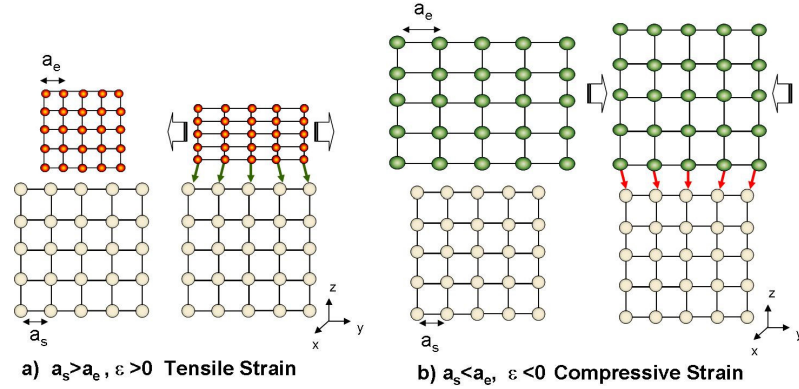


**Figure 2.6** Schematic diagram (a) tensile-strained and (b) compressively-strained layers grown on thick substrates [30].

In compressive strain  $a_s < a_e$ ,  $\varepsilon_{xx} = \varepsilon_{yy} < 0$  and,  $\varepsilon_{zz} > 0$ , for tensile strain  $a_s > a_e$ ,  $\varepsilon_{xx} = \varepsilon_{yy} > 0$  and  $\varepsilon_{zz} < 0$ .

The total strain can be determined by using axial component,  $\varepsilon_{ax}$ :

$$\varepsilon_{ax} = \varepsilon_{\perp} - \varepsilon_{\parallel} \approx 2\varepsilon_{\parallel} \quad (2.29)$$

and the hydrostatic component  $\varepsilon_{vol} = \Delta V/V$ , given by:

$$\varepsilon_{vol} = \varepsilon_{xx} + \varepsilon_{yy} + \varepsilon_{zz} \approx \varepsilon_{\parallel} \quad (2.30)$$

When modelling the effects of strain on the band structure of semiconductors, the strain curve is important. Figure 2.7 compares the compressive and tensile strained structures with unstrained case,

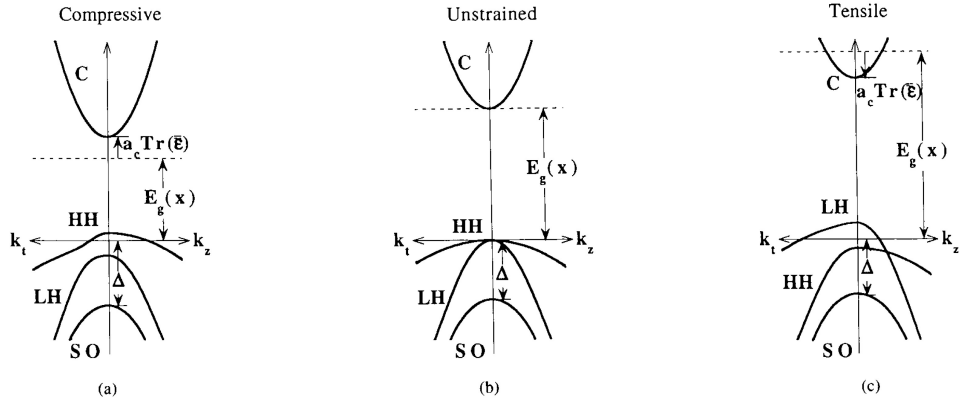


**Figure 2.7** Schematic diagram showing the bulk band structure of three  $\text{In}_{1-x}\text{Ga}_x\text{As}$  ternary strained layers grown on InP substrate [31].

## 2.5 Summary

In this chapter, we give a brief theoretical review of band anti-crossing models and strain theory that we require for III-V nitride and bismide material systems used throughout this thesis.

## CHAPTER 3

### CALCULATION OF BAND STRUCTURE OF INDIUM BASED III-V BISMIDES ALLOYS

#### 3.1 Introduction

$\text{InSb}_{1-x}\text{Bi}_x$  and  $\text{InAs}_{1-x}\text{Bi}_x$  are narrow gap semiconductors and they emit light in 3-5 and 8-12  $\mu\text{m}$  range of wavelengths. Thus, these semiconductors can be used for applications in infrared detectors [32].  $\text{InP}_{1-x}\text{Bi}_x$  is a medium forbidden gap semiconductor. Its broad emission wavelength corresponds to the telecommunication wavelengths in infrared region. The introduction of Bi reduces the temperature dependence of the energy  $E_g$  of bismide alloys allowing to grow photonic devices having temperature insensitive emission wavelengths. Since Bi related impurity states are far away from conduction band edge, there is a little perturbation in CB. Thus the effective mass of electron is not influenced effectively. This cause a less degradation in mobility of electron in bismide alloys compared to nitride alloys [33, 34].

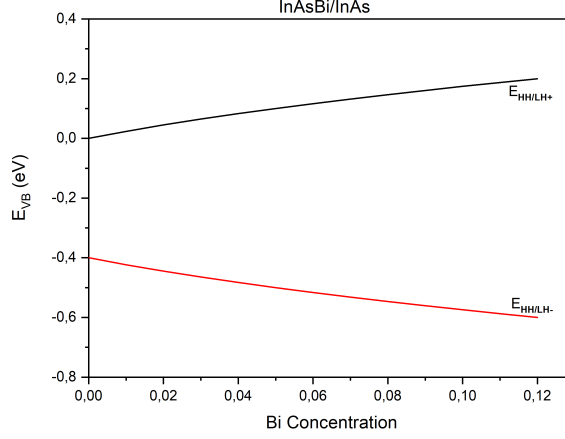
Incorporation of bismuth atoms into the binary InAs, InP and InSb III-V host semiconductor materials, introduces localized bismuth energy levels near the VBE of the host binary semiconductor materials. These bismuth energy levels interact with the extended states of the III-V host semiconductor materials leading a splitting in VB into  $E_+$  and  $E_-$ . We use V-BAC model to investigate the interaction between bismuth energy levels and the extended states. The necessary material parameters are given in the Table 3.1.

**Table 3.1** The material parameters for ternary materials [4, 13, 26, 35].

Material	InAs <sub>1-x</sub> Bi <sub>x</sub>	InSb <sub>1-x</sub> Bi <sub>x</sub>	InP <sub>1-x</sub> Bi <sub>x</sub>	GaAs <sub>1-x</sub> Bi <sub>x</sub>
$\gamma_1$	20.0	34.8	5.08	6.98
$\gamma_2$	8.5	15.5	1.6	2.06
$\gamma_3$	9.2	16.5	2.1	2.93
$\Delta_0$ (eV)	0.39	0.81	0.108	0.34
$\Delta E_{CBM}$ (eV)	-1.03	-1.44	-1.74	-2.3
$\Delta E_{VBM}$ (eV)	0.94	0.35	1.3	0.6
$E_{Bi-so}$ (eV)	1.9	2.5	1.6	2.2
$\Delta E_{SO}$ (eV)	-0.87	-1.04	-0.69	-1.3
$E_{Bi}$ (eV)	0.4	1.0	0.1	0.4
$C_{Bi}$ (eV)	1.0	1.33	0.5	1.6

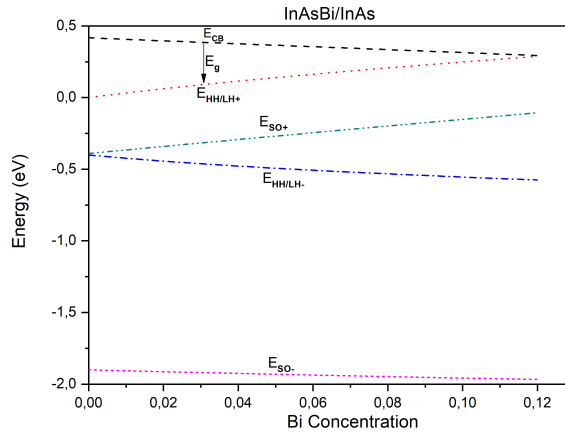
### 3.2 InAs<sub>0.88</sub>Bi<sub>0.12</sub>

In this section, we have presented to the incorporation of Bi into the InAs host semiconductor materials. Incorporation of a small amount of bismuth atoms into the binary III-V host semiconductor materials produces 'dilute bismides'. Alloying a small amount of bismuth atoms into InAs host material provides long wavelength infrared photo-detectors [36] and lasers [37]. The VBE of InAs<sub>1-x</sub>Bi<sub>x</sub> is expressed as a function of Bi concentration  $x$  using the V-BAC model [13] in equation 2.10. Table 3.1 presents the required parameters for ternary materials in our calculations.  $E_{Bi}$  shows the position of the  $E_{HH/LH}$  levels for bismide which is located 400 meV below VB maximum of InAs.  $E_{Bi-SO}$  indicates the location of spin-orbit splitt-off level that is located 1.9 eV below the VB maximum of the host InAs.  $C_{Bi}$  is the fitting parameter obtained from experimental values. The incorporation of bismide into InAs leads a composition dependent BAC interaction between the VBE states of host InAs and localized Bi impurity states. The results of bismuth induced band mixing due to hybridisation of valence states is presented in figure 3.1 for the energy locations of  $E_+$  and  $E_-$  energy levels of the heavy hole and light hole. The heavy hole and light hole coincide with each other at  $\Gamma$  point. Figure 3.1 shows the variations of these energy locations of  $E_+$  and  $E_-$  for  $E_{HH/LH}$ . The upper subband  $E_{HH/LH+}$  increase with increasing dilute bismide concentration, but the lower subband  $E_{HH/LH-}$  of valence band decrease with increasing dilute bismide concentration. The increase in upper subband  $E_{HH/LH+}$  with incorporated bismide concentration cause a decrease in bandgap reduction.



**Figure 3.1** Variation of relative energy locations for  $E_{HH/LH+}$  and  $E_{HH/LH-}$  as a function of Bi concentration for  $\text{InAs}_{1-x}\text{Bi}_x$  on InAs.

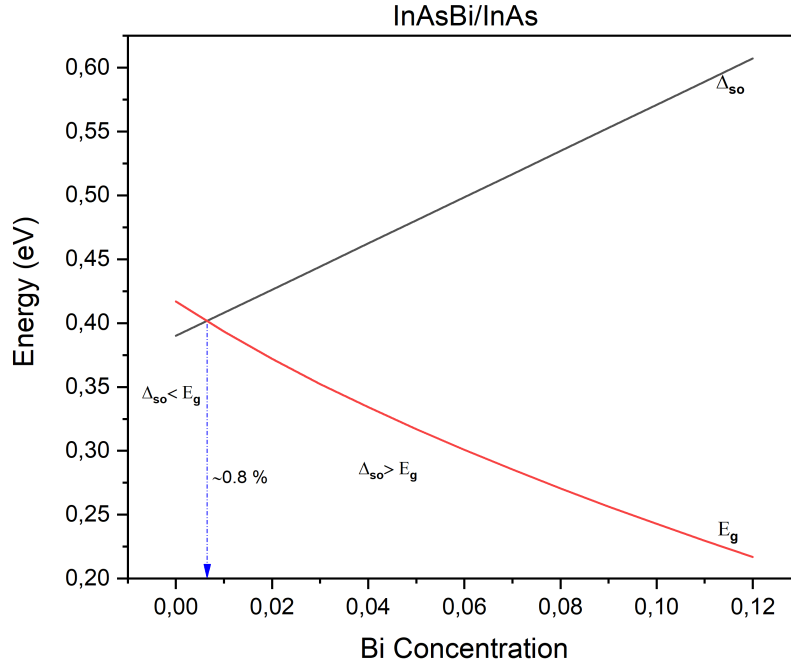
Figure 3.2 illustrates the repulsive interaction between the light hole, heavy hole and split off band of  $E_+$  and  $E_-$  energy levels of InAsBi. The  $E_{HH/LH+}$  level increases at the rate of 32.5 meV per Bi concentration and the  $E_{SO+}$  energy level increases by 24.6 meV per Bi incorporation in the alloy. Figure 3.2 also shows that  $E_{CB}$  goes in downward direction by increasing bismuth concentration and this reduction is 10.3 meV per Bi concentration as predicted by virtual crystal approximation, VCA, model. As an overall, there is a calculated value of 42.8 meV per percent of Bi concentration. This value is in good agreement with Samajdar et al. [25].



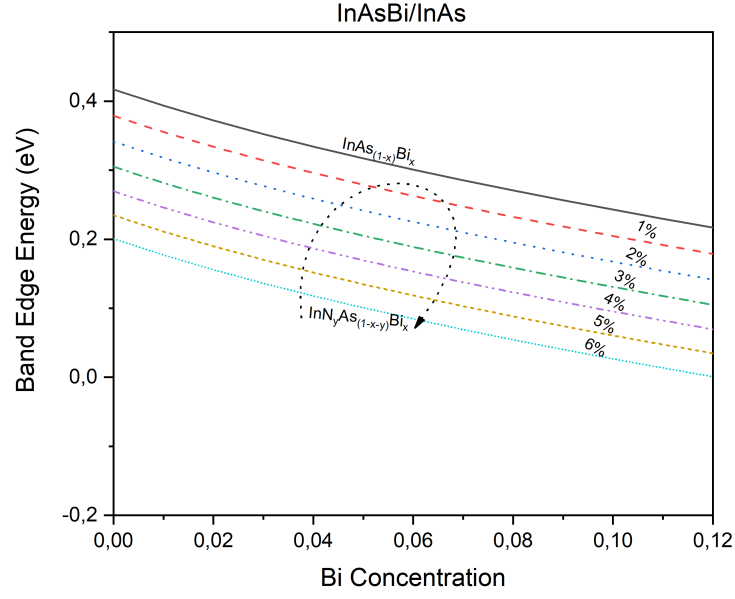
**Figure 3.2** Energy locations  $E_+$  and  $E_-$  of the heavy hole, light hole and split-off bands for  $\text{InAs}_{1-x}\text{Bi}_x/\text{InAs}$  as a function of Bi concentration up to 12 %.

Figure 3.3 presents the total reduction in  $E_g$  and the rate of change of  $\Delta_0$  as a function of bismide concentration. These variations illustrate how  $E_g$  and  $\Delta_0$  vary relative to one another with incorporated bismide concentration. The main purpose of these calculations is to determine at which point, i.e concentration,  $E_g$  and  $\Delta_0$  coincide. As it is seen from Figure 3.3, when small fraction of bismuth atoms  $\approx 0.8\%$  are incorporated, the energy of spin-orbit splitting,  $\Delta_0$  crosses over the band gap energy,  $E_g$  and after  $\approx 0.8\%$  bismuth concentration,  $\Delta_0 > E_g$ . This means that optical loss mechanisms can be eliminated by using only  $\approx 0.8\%$  bismuth concentration.

Moreover, we try to reveal the effect of N concentration in  $\text{InAs}_{1-x}\text{Bi}_x$  with various concentration of N (up to 6%). Our calculated results have been illustrated in Figure 3.4. The calculated values shown in figure 3.4 clearly shows that the incorporation of N into InAsBi causes further reductions in energy band gap. We have used  $E_g$  of InBi 1.62 eV [38] and  $\Delta_0$  as 2.2 eV [39].



**Figure 3.3** Variation of  $E_g$  and  $\Delta_0$  as a function of Bi concentration for  $\text{InAs}_{1-x}\text{Bi}_x/\text{InAs}$ .



**Figure 3.4** Estimated variation of band edge energy due to Bi (up to 12 %) and N (up to 6 %) incorporation in  $\text{InAs}_{1-x-y}\text{N}_y\text{Bi}_x$  on InAs substrates.

The in-plane strain along x and y directions for  $\text{InAs}_{1-x}\text{Bi}_x/\text{InAs}$  is defined by

$$\varepsilon_{\parallel} = \frac{a_{\text{InAs}} - a_{\text{InAsBi}}}{a_{\text{InAsBi}}} \quad (3.1)$$

where  $a_{\text{InAsBi}}$  is the lattice constant of ternary InBiAs and  $a_{\text{InBi}} = 6.686 \text{ \AA}$  is the lattice constant of substrate [39]. The lattice constant of ternary material can be calculated by means of using the Vegards law;

$$a_{\text{InAs}_{1-x}\text{Bi}_x} = (1 - x) \cdot a_{\text{InAs}} + x \cdot a_{\text{InBi}} \quad (3.2)$$

The strain along the growth z-direction is defined by

$$\varepsilon_{\perp} = -\left(\frac{2C_{12}}{C_{11}}\right)\varepsilon_{\parallel} \quad (3.3)$$

where  $C_{11}$  and  $C_{12}$  are the elastic constants of  $\text{InAs}_{1-x}\text{Bi}_x$ . The corresponding calculated strain values have been presented in Figures 3.5 and 3.6. The strain along the growth direction increases with an increasing bismuth concentration and the strain is tension, however the strain along the in-plane directions is compressive and also increases with increasing bismuth concentration. When  $\text{InAs}_{1-x}\text{Bi}_x$  is grown on a InAs the in-plane strain is compressive while for  $\text{InN}_y\text{As}_{1-x-y}\text{Bi}_x$  it is tensile. This is due to the fact that nitrogen and bismide have opposite effects on the lattice constant. Figure 3.6 clearly shows that the introduction of N

into InAsBi decreases the magnitude of compressive strain. The quaternary alloy  $\text{InN}_y\text{As}_{1-x-y}\text{Bi}_x$ , therefore, allows to control strain and tune the bandgap for operation wavelengths of 3-5  $\mu\text{m}$ . The necessary material parameters are given in the Table 3.2.

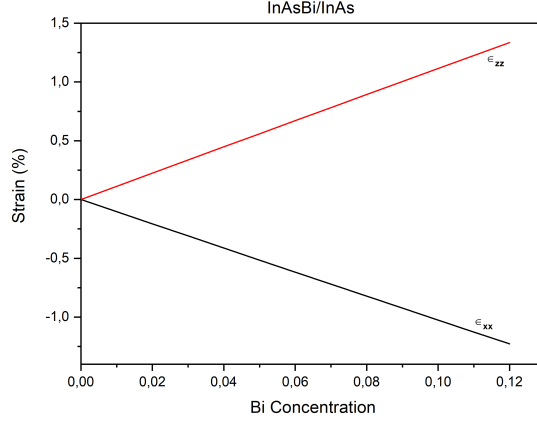


**Figure 3.5** The strain along the growth x and z direction versus bismuth concentration in the  $\text{InAs}_{1-x}\text{Bi}_x/\text{InAs}$ .

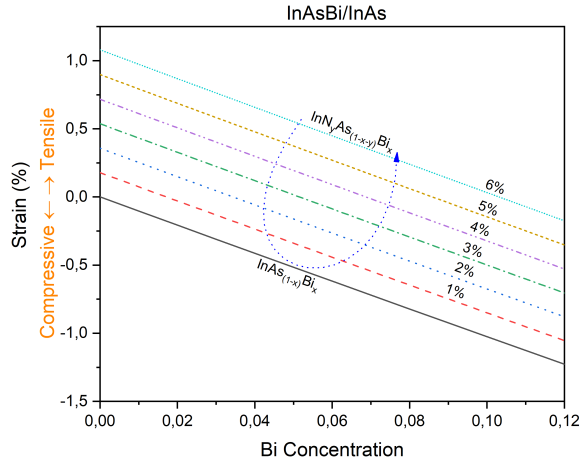


**Figure 3.6** Estimated variation of strain due to Bi (up to 12 %) and N (up to 6 %) incorporation in  $\text{InAs}_{1-x}\text{Bi}_x$  and  $\text{InN}_y\text{As}_{1-x-y}\text{Bi}_x$  on InAs substrates.

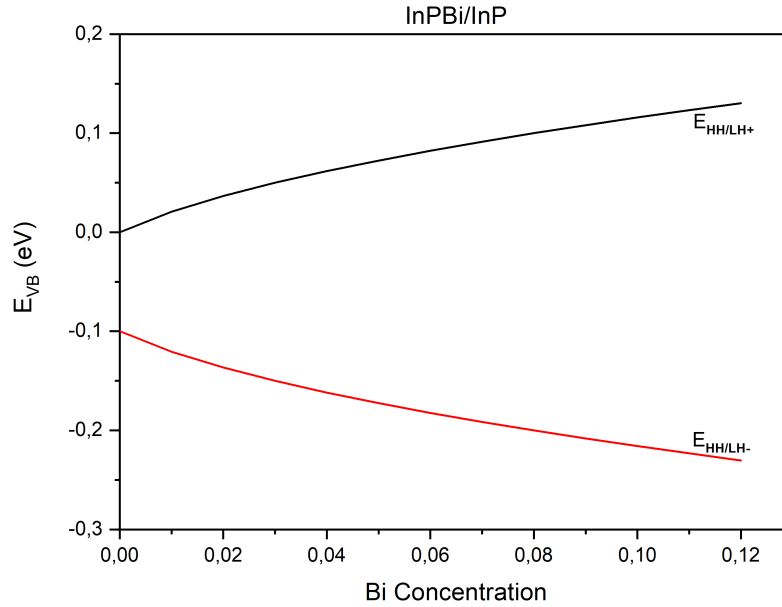
**Table 3.2** The lattice constants used in our calculations for binary materials [26, 39].

Material	InAs	InSb	InP	InBi
Lattice Constant $a_0$ (Å)	6.0583	6.4794	5.8697	6.686

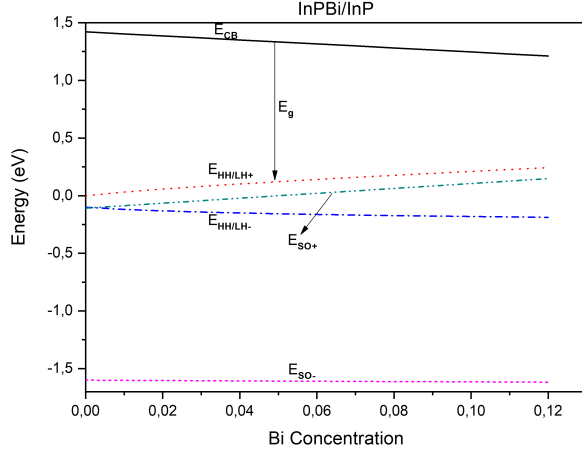


### 3.3 $\text{InP}_{0.88}\text{Bi}_{0.12}$

Incorporation of Bi into InP host semiconductor materials produces InPBi material. Group III-V semiconductors phosphides (P) are important materials for optoelectronic devices operating at visible and near-infrared wavelength range [40, 41]. The incorporation of a small concentration Bi into InP host material can increase the wavelengths for optoelectronic materials leading an improved device performances. Berding et al. [42] theoretically examined InSbBi, InAsBi and InPBi materials; and stated that InSbBi was the simplest material system. He also stated that InPBi was the most difficult material system than the others due to its larger band gap compared to that of InAsBi and InSbBi materials [42]. The incorporation of bismide into InP leads a composition dependent BAC interaction between the VBE states of host InP and localized Bi impurity states. Figure 3.7 shows the variations of these energy locations of  $E_+$  and  $E_-$  for  $E_{HH/LH}$  as a function of Bi concentration. The upper subband  $E_{HH/LH+}$  increase with increasing dilute bismide concentration, but the lower subband  $E_{HH/LH-}$  of VB decrease with increasing dilute bismide concentration. Figure 3.8 shows the variations of the heavy hole, light hole and split-off bands of  $E_+$  and  $E_-$  energy levels with bismuth concentration.

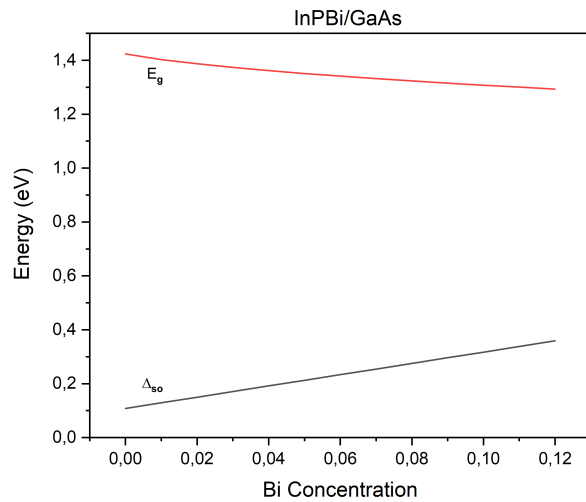


**Figure 3.7** Variation of relative energy locations for  $E_{HH/LH+}$  and  $E_{HH/LH-}$  as a function of Bi concentration for  $\text{InP}_{1-x}\text{Bi}_x$  on InP substrates.



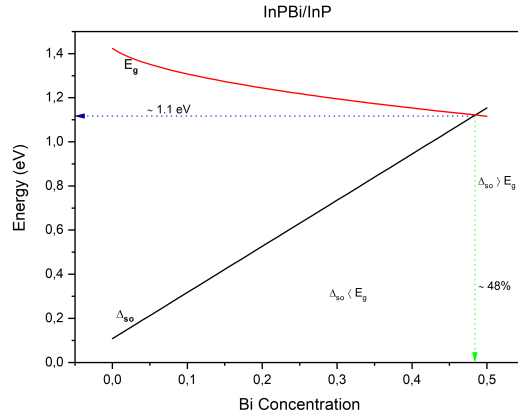
**Figure 3.8** Energy locations  $E_+$  and  $E_-$  of the heavy hole, light hole and split-off bands for  $\text{InP}_{1-x}\text{Bi}_x/\text{InP}$  as a function of Bi concentration up to 12 %.

Figure 3.8 illustrates that the  $E_{HH/LH+}$  level increases at a rate of 31.9 meV per Bi concentration and the  $E_{SO+}$  energy level increases by 21.7 meV per Bi incorporation in the alloy. However  $E_{CB}$  level decreases by 17.4 meV. The values of  $\Delta_0$  of  $\text{InP}_{1-x}\text{Bi}_x$  are too small compared to  $E_g$ . Therefore,  $E_g$  energy and  $\Delta_0$  does not cross over until bismuth concentration is up to 48 %. This means that one cannot suppress or eliminate optical loss mechanism unless a bismuth concentration in the order of 48 % is not incorporated to InP. Figure 3.9 shows the rate of change of the  $E_g$  and  $\Delta_0$  versus bismuth concentration.



**Figure 3.9** Variation of  $E_g$  and  $\Delta_0$  as a function of Bi concentration for  $\text{InP}_{1-x}\text{Bi}_x/\text{InP}$ .

As can be seen from figure 3.10, when 48 % bismuth concentration are incorporated into InP host material, the values of  $\Delta_0$  and  $E_g$  gets closer to each other and after 48 % bismuth concentration  $\Delta_0$  and  $E_g$  crosses over each other and beyond this concentration  $\Delta_0$  becomes greater than  $E_g$ . Thus when bismuth concentration is greater than 48 %, both Auger recombination and Intervallence band absorption is expected to be eliminated. Figure 3.10 also illustrates that the  $\Delta_0$  level increases at the rate of  $\approx 20.9$  meV per Bi concentration and the  $E_g$  energy level decreases by  $\approx 20.7$  meV per Bi incorporation in the alloy. The additional effect of nitrogen on  $E_g$  reduction is illustrated in figure 3.11. These results clearly show how the incorporation of nitrogen into InPBi cause a rapid reduction in energy  $E_g$  allowing to tune the wavelength effectively.



**Figure 3.10** Variation of  $E_g$  and  $\Delta_0$  as a function of Bi concentration for  $\text{InP}_{1-x}\text{Bi}_x/\text{InP}$ .

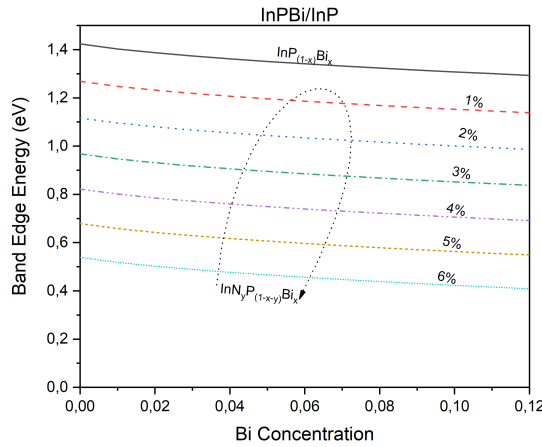


**Figure 3.11** Estimated variation of band edge energy due to Bi (up to 12 %) and N (up to 6 %) incorporation in  $\text{InP}_{1-x-y}\text{N}_y\text{Bi}_x$  on InP substrates.

The in-plane strain along the x and y directions for  $\text{InP}_{1-x}\text{Bi}_x/\text{InP}$  is defined by

$$\varepsilon_{\parallel} = \frac{a_{\text{InP}} - a_{\text{InPBi}}}{a_{\text{InPBi}}} \quad (3.4)$$

where  $a_{\text{InPBi}}$  is the lattice constant of ternary InPBi material can be calculated by means of using the Vegards law;

$$a_{\text{InP}_{1-x}\text{Bi}_x} = (1 - x) \cdot a_{\text{InP}} + x \cdot a_{\text{InBi}} \quad (3.5)$$

The strain along the growth z-direction is defined by

$$\varepsilon_{\perp} = -\left(\frac{2C_{12}}{C_{11}}\right)\varepsilon_{\parallel} \quad (3.6)$$

where  $C_{11}$  and  $C_{12}$  are the elastic constants of  $\text{InP}_{1-x}\text{Bi}_x$ . The strain along the growth direction increases with an increasing bismuth concentration and the strain along the in-plane direction increases with opposite signs with increasing bismuth concentration. When  $\text{InP}_{1-x}\text{Bi}_x$  is grown on a InP the strain is compressive while for  $\text{InN}_y\text{P}_{1-x-y}\text{Bi}_x$  is a tensile strain. The corresponding strain values have been presented in Figures 3.12 and 3.13.

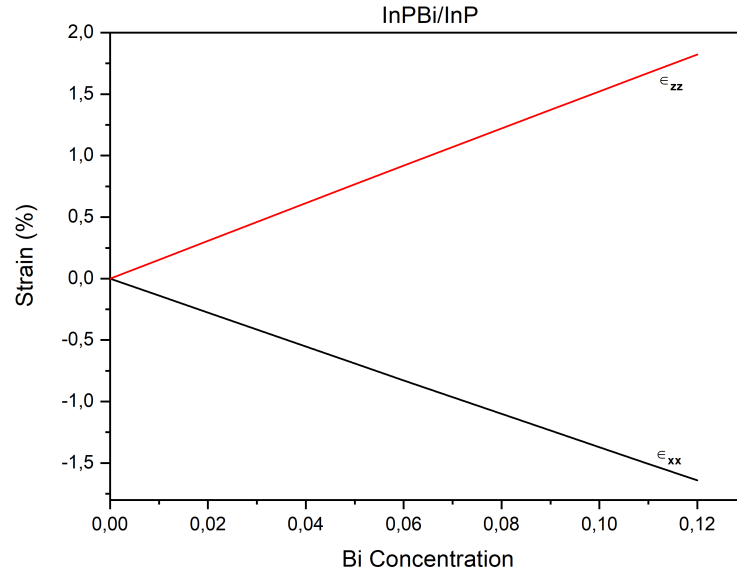


**Figure 3.12** The strain along the growth x and z direction versus bismuth concentration in  $\text{InP}_{1-x}\text{Bi}_x/\text{InP}$ .

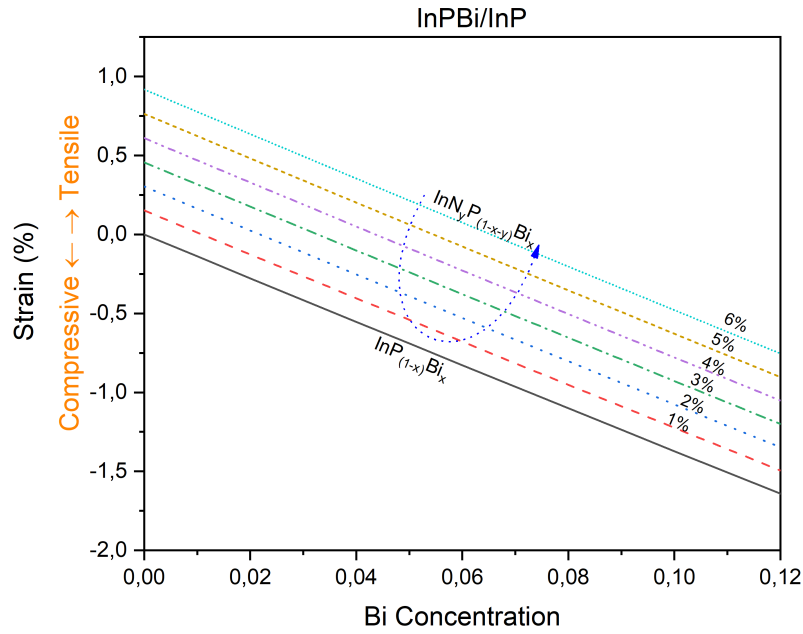


**Figure 3.13** Estimated variation of strain due to Bi (up to 12 %) and N (up to 6 %) incorporation in  $\text{InP}_{1-x}\text{Bi}_{0.x}$  and  $\text{InN}_y\text{P}_{1-x-y}\text{Bi}_x$  on InP substrates.

### 3.4 $\text{InSb}_{0.88}\text{Bi}_{0.12}$

Incorporation of Bi atoms into InSb host semiconductor material produces dilute bismide InSb material. This incorporation leads a composition dependent BAC interaction between the VBE states of host InSb and localized Bi impurity states. The results of bismuth induced band mixing due to hybridisation of valence states is presented in figure 3.14 for the energy locations of  $E_+$  and  $E_-$  energy levels for HH/LH. The heavy hole and light hole coincide with each other at  $\Gamma$  point. Figure 3.14 illustrates that the upper subband  $E_{HH/LH+}$  increase with increasing dilute bismide concentration, but the lower subband  $E_{HH/LH-}$  of VB decrease with increasing dilute bismide concentration as in the case of previously examined dilute bismide alloys..

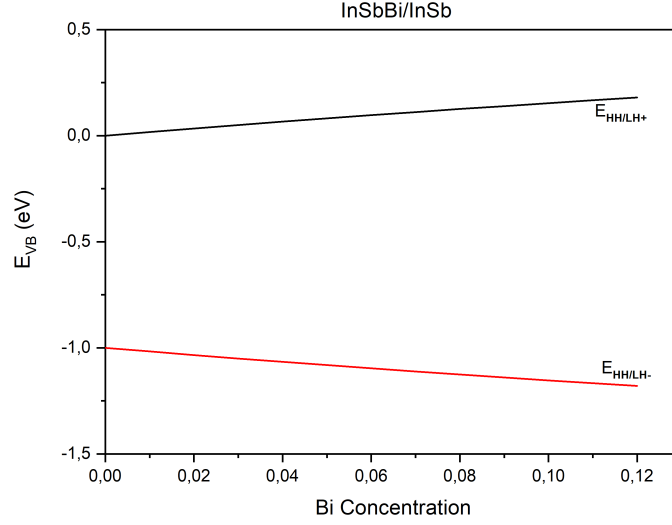


**Figure 3.14** Variation of relative energy locations for  $E_{HH/LH+}$  and  $E_{HH/LH-}$  as a function of Bi concentration for  $\text{InSb}_{1-x}\text{Bi}_x$  on InSb substrates.

InSb is a narrow gap semiconductor with an energy  $E_g$  of 0.235 eV and  $\Delta_0$  energy of 0.81 eV[26]. The calculated values of  $\Delta_0$  and  $E_g$  for ternary  $\text{InSb}_{1-x}\text{Bi}_x$  is shown in figure 3.15. There is no rapid  $E_g$  reduction and strong  $\Delta_0$  for  $\text{InSb}_{1-x}\text{Bi}_x$  due to the values of  $\Delta_0$  and  $E_g$  of InSb host material. According to our calculations  $E_g$  energy and  $\Delta_0$  never crosses since the value of  $\Delta_0$  is much bigger than the  $E_g$ .

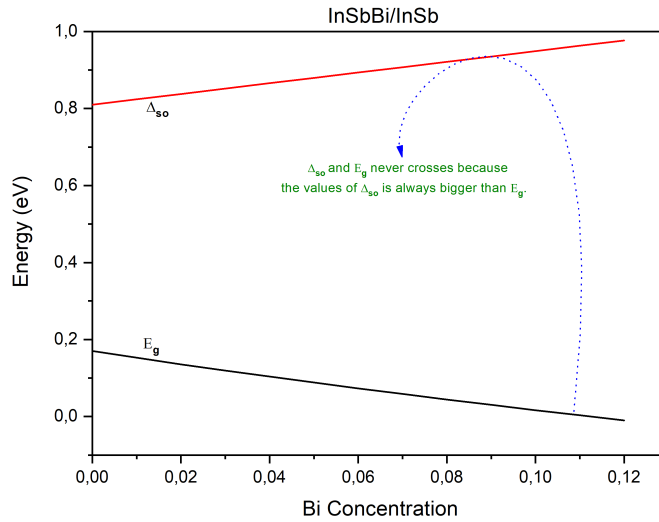


**Figure 3.15** Variation of  $E_g$  and  $\Delta_0$  as a function of Bi concentration for  $\text{InSb}_{1-x}\text{Bi}_x/\text{InSb}$ .

The energy locations of the  $E_+$  and  $E_-$  energy levels of the light hole, heavy hole and split off band as functions of bismuth concentration up to 12 % is given in figure 3.16. The calculations presented here illustrates that the  $E_{HH/LH+}$  and  $E_{SO+}$  level increases at a rate of 20.8 meV and 24.2 meV per Bi concentration, however  $E_{CB}$  level decreases by 14.4 meV, respectively. As can also be seen from figure 3.16 the theoretical  $E_g$  of  $\text{InSb}_{1-x}\text{Bi}_x$  reduces to zero for  $\approx 5\%$  Bi concentration.

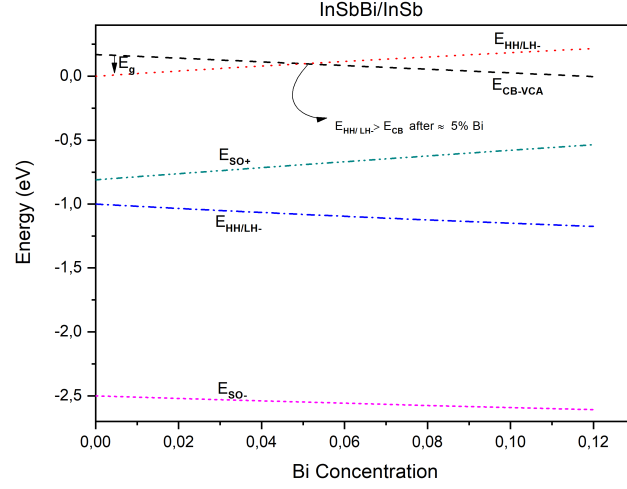


**Figure 3.16** Energy locations  $E_+$  and  $E_-$  of the heavy hole, light hole and split-off bands for  $\text{InSb}_{1-x}\text{Bi}_x/\text{InSb}$  as a function of Bi concentration up to 12 %.

The in-plane strain along the x and y directions for  $\text{InSb}_{1-x}\text{Bi}_x/\text{InSb}$  is defined by

$$\varepsilon_{\parallel} = \frac{a_{\text{InSb}} - a_{\text{InSbBi}}}{a_{\text{InSbBi}}} \quad (3.7)$$

where  $a_{\text{InSbBi}}$  is the lattice constant of ternary  $\text{InSbBi}$  material can be calculated by means of using the Vegards law;

$$a_{\text{InSb}_{1-x}\text{Bi}_x} = (1 - x) \cdot a_{\text{InSb}} + x \cdot a_{\text{InBi}} \quad (3.8)$$

The strain along the growth z-direction is defined by

$$\varepsilon_{\perp} = -\left(\frac{2C_{12}}{C_{11}}\right)\varepsilon_{\parallel} \quad (3.9)$$

where  $C_{11}$  and  $C_{12}$  are the elastic constants of  $\text{InSb}_{1-x}\text{Bi}_x$ . The strain along z-direction increases with an increasing bismuth concentration and the strain along the growth direction increases opposite directions with increasing bismuth

concentration. When  $\text{InSb}_{1-x}\text{Bi}_x$  is grown on an InSb substrate the strain is compressive while for  $\text{InN}_y\text{Sb}_{1-x-y}\text{Bi}_x$  it is a tensile strain. The corresponding strain values have been presented in Figures 3.17 and 3.18.

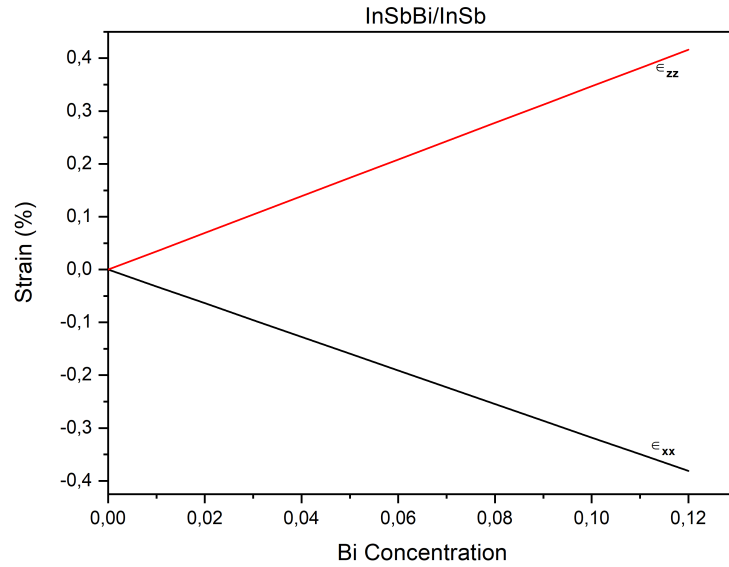


**Figure 3.17** The strain along the growth x and z direction versus bismuth concentration in the  $\text{InSb}_{1-x}\text{Bi}_x/\text{InSb}$ .

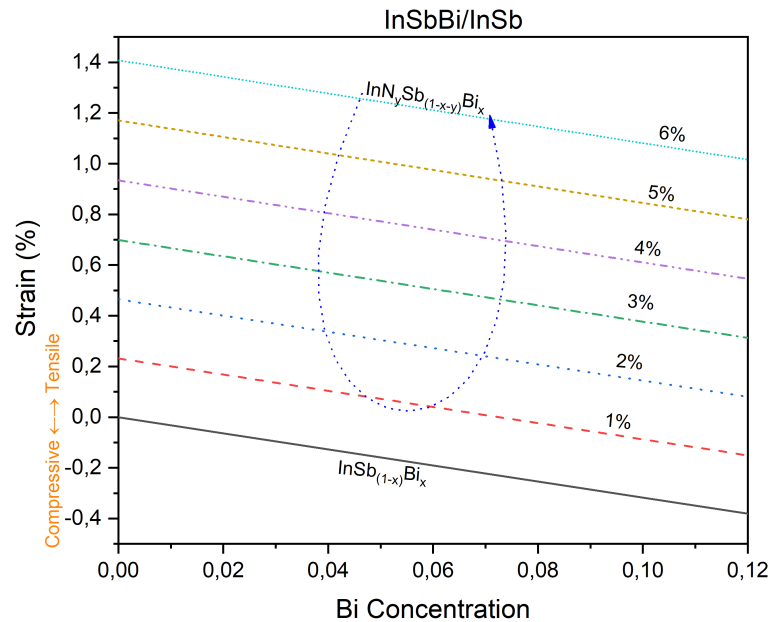


**Figure 3.18** Estimated variation of strain due to Bi (up to 12 %) and N (up to 6 %) incorporation in  $\text{InSb}_{1-x}\text{Bi}_x/\text{InSb}$  and  $\text{InN}_y\text{Sb}_{1-x-y}\text{Bi}_x$  on InSb substrates.



### 3.5 Summary

In this chapter, we have presented an analysis of electronic band structure of ternary  $\text{InAs}_{1-x}\text{Bi}_x/\text{InAs}$ ,  $\text{InP}_{1-x}\text{Bi}_x/\text{InP}$  and  $\text{InSb}_{1-x}\text{Bi}_x/\text{InSb}$  materials by using valence band anti-crossing model, V-BAC. Our calculated results show that  $E_g$  decreases and  $\Delta_0$  increases with increasing bismuth concentration. The rate of change of these values vary from one material to another. We have shown that  $E_g$  and  $\Delta_0$  cross over at different bismuth concentration for each material system due to their band gap and  $\Delta_0$  difference. We have calculated that  $\Delta_0$  becomes greater than  $E_g$  for  $\approx 0.8\%$  bismuth concentration for  $\text{InAs}_{1-x}\text{Bi}_x/\text{InAs}$  material system. It has been calculated that in order to achieve a crossover of  $E_g$  with  $\Delta_0$ , a bismuth concentration in the order of  $50\%$  is required for  $\text{InP}_{1-x}\text{Bi}_x/\text{InP}$  alloy system. On the other hand, there is no need to increase bismuth concentration for  $\text{InSb}_{1-x}\text{Bi}_x$  to achieve  $\Delta_0 > E_g$  since it is already satisfied.

## CHAPTER 4

### CALCULATION OF BAND STRUCTURE OF ARSENIDE BASED III-V DILUTE BISMIDES AND NITRIDES

#### 4.1 Introduction

There is a steadily increasing interest in highly mismatch alloys of III-V nitrides and bismides due to their unusual band structures. These unusual behaviour is a result of the composition dependent bowing due to the impurity like behaviour of isovalent atoms with the respective band edges. In this chapter, we try to reveal the change in band structure when N and Bi atom is introduced to the arsenide based III-V compound semiconductors of GaAsBi, GaAsN and GaAsNBi.

#### 4.2 GaAs<sub>0.88</sub>Bi<sub>0.12</sub>

There is a growing attention in incorporation of bismuth atoms into III-V GaAs host materials, due to their potential as an interesting band structure. This material system can be considered as a promising candidate for long-wavelength device applications, next generation multijunction solar cells [43], long wavelength light emitters [44, 45], transistors [46] and spintronic devices [47] due to their optimal band structure properties. When a small concentration of As is replaced by Bi atoms in GaAs host material, the energy gap,  $E_g$  decreases rapidly i.e. there is approximately 60 meV reduction for 1% of replaced Bi atoms [48]. Photo-reflectance measurements show that  $\Delta_0$  increases rapidly with Bi concentration as well [28].

The incorporation of Bi atom into III-V GaAs host material was first proposed by Oe et al in 1998 [49]. Oe et al has suggested the compound GaAs<sub>1-y</sub>Bi<sub>y</sub> which is called as a dilute bismide alloy is constructed from a binary GaAs semiconductor and a semi-metal GaBi materials [49]. The resultant dilute bismide cause  $E_g$  reduction and an increase in  $\Delta_0$ . The  $E_g$  reduction is expected due to semi-metallic

character of GaBi [50]. The band structure of GaAsBi can also be explained in terms of V-BAC model [23, 51, 52].

A localized impurity bismuth energy level is introduced into the VB of host GaAs. As a result of valence band anti-crossing, valence band splits into two characteristic subbands  $E_+$  and  $E_-$  energy levels of HH/LH. The heavy hole and light hole coincide with each other at  $\Gamma$  point. Figure 4.1 shows the variations of these energy positions of  $E_+$  and  $E_-$  for  $E_{HH/LH}$ . These variations show that the rate of splitting gets bigger with increasing Bi concentration. The upper subband  $E_{HH/LH+}$  increase with increasing dilute bismide concentration, but the lower subband  $E_{HH/LH-}$  of VB decrease with increasing dilute bismide concentration. However  $E_{CB}$  level decreases by 23.0 meV. The increase in upper subband  $E_{HH/LH+}$  with incorporated bismide concentration cause a decrease in  $E_g$  reduction similar to the results that we have obtained in chapter 3.

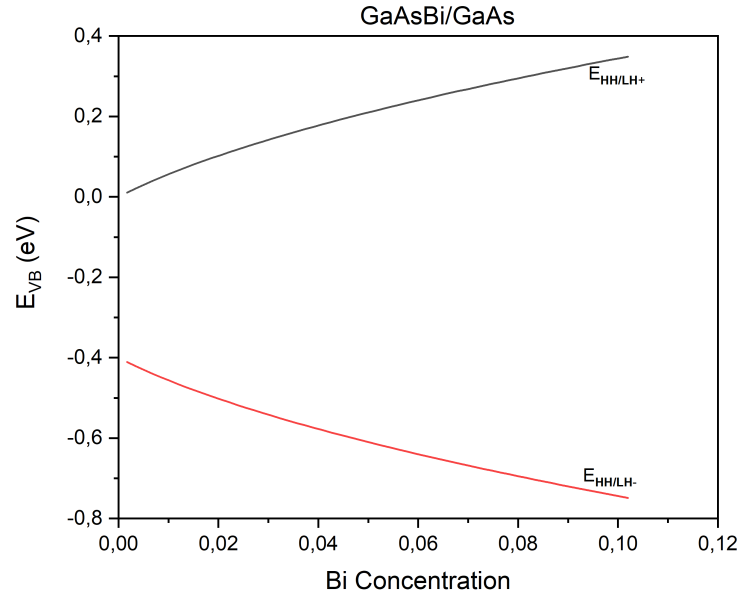


**Figure 4.1** Variation of relative energy positions for  $E_{HH/LH+}$  and  $E_{HH/LH-}$  as a function of Bi concentration for  $\text{GaAs}_{1-y}\text{Bi}_y$  on GaAs substrates.

Like arsenide (As), bismuth (Bi) is also a group-V element and atomic radius of Bi is much larger than that of As. As a result of their atomic size difference, bismide atoms behave as an impurity and these atoms occupy at an energy level just below the VB. Thus the BAC interaction is expected between the Bi impurity energy levels and the VBE of the GaAs host material [53]. The interaction of Bi impurity energy level with VBE; produces a new VB maximum corresponding

to  $E_{HH/LH+}$ . However there have been no experimental results of the  $E_{HH/LH-}$  band [5]. The upward movement of the VBE of GaAsBi alloy due to anti-crossing interaction presents a  $E_g$  reduction.

Due to anti-crossing interaction VB also splits into six valence subbands, which may be classified into the heavy hole, light hole and split-off bands with a series of  $E_+$  and  $E_-$  subbands energy levels due to BAC model [13]. Figure 4.2 shows the variations of these relative energy locations of  $E_+$  and  $E_-$  energy levels for the heavy hole, light hole and split-off bands with Bi concentration up to 12 %. Our calculated results indicates that the  $E_{HH/LH+}$  and  $E_{SO+}$  level increases at the rate of  $\approx 61.5$  meV and  $\approx 32.5$  meV per Bi concentration in the alloy, respectively.

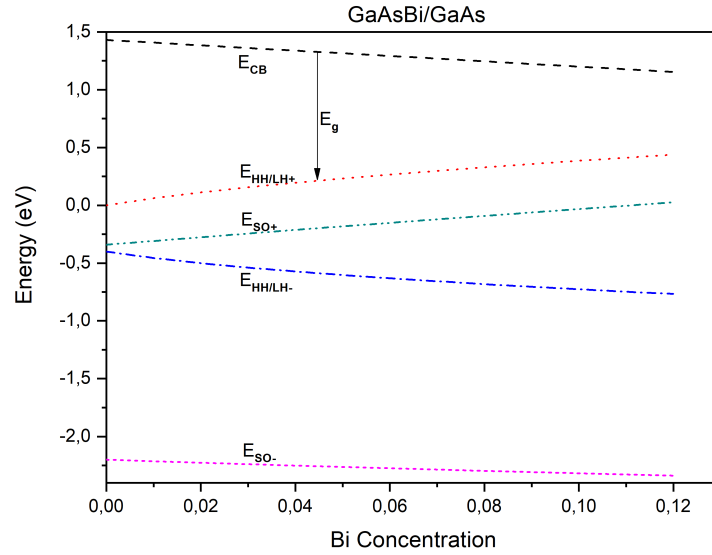


**Figure 4.2** Energy locations  $E_+$  and  $E_-$  of the heavy hole, light hole and split-off bands for  $\text{GaAs}_{1-y}\text{Bi}_y/\text{GaAs}$  as a function of Bi concentration up to 12 %.

Binary GaBi is predicted to have a large  $\Delta_0$  of 2.2 eV [6] compared to that of GaAs host. When incorporated Bi concentration is greater 10%, the  $\Delta_0$  becomes greater than the  $E_g$  energy [8, 28, 48, 54]. This situation of  $\Delta_0 > E_g$  prohibits the optical loss mechanisms [10].

We use V-BAC model to investigate the interaction between bismuth impurity energy levels and the extended host GaAs states. The calculated result according to this model; indicates a rapid reduction in  $E_g$  and a remarkable increase of the  $\Delta_0$  with increasing Bi concentration. Figure 4.3 presents the total reduction in  $E_g$  and the rate of change of  $\Delta_0$  as a function of bismide concentration. The results presented in Figure 4.3 shows that  $E_g$  and  $\Delta_0$  opposes each other with increasing

bismide concentration. By means of these calculation we would like to determine at which point  $E_g$  and  $\Delta_0$  coincide. As it is seen from Figure 4.3, when fraction of bismuth atoms in the order of 9.7 % are incorporated, the energy of  $\Delta_0$  crosses over the  $E_g$  energy and beyond this value bismuth concentration,  $\Delta_0 > E_g$ . Thus optical loss mechanisms can be eliminated by using bismuth concentration in the order of 9.7 %. In this dilute bismide alloy,  $E_g$  decreases by 15.36 meV per Bi concentration, while  $\Delta_0$  increases  $\approx 13.0$  meV per Bi concentration.

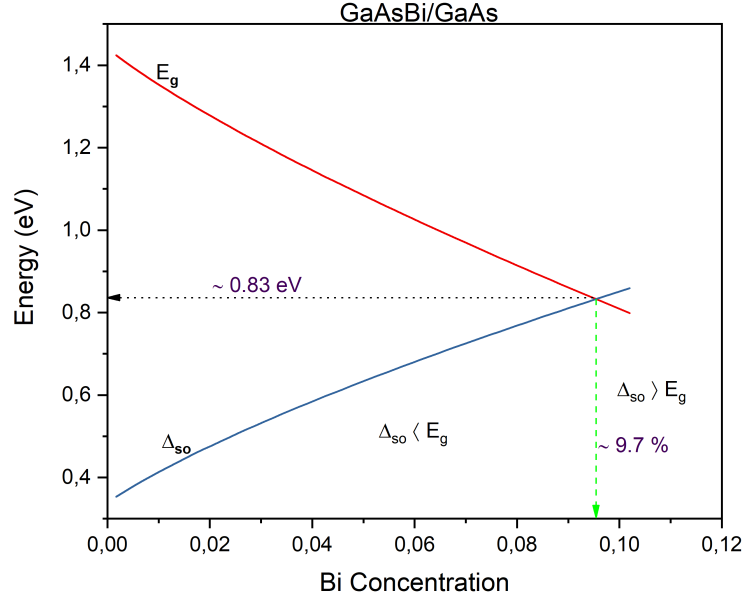


**Figure 4.3** Variation of  $E_g$  and  $\Delta_0$  as a function of Bi concentration for  $\text{GaAs}_{1-y}\text{Bi}_y/\text{GaAs}$ .

The strain along the x and y directions for  $\text{GaAs}_{1-y}\text{Bi}_y/\text{GaAs}$  is defined by

$$\varepsilon_{\parallel} = \frac{a_{\text{GaAs}} - a_{\text{GaBiAs}}}{a_{\text{GaBiAs}}} \quad (4.1)$$

where  $a_{\text{GaAsBi}}$  is the lattice constant of ternary GaBiAs material can be calculated by means of using the Vegards law;

$$a_{\text{GaAs}_{1-y}\text{Bi}_y} = (1 - y) \cdot a_{\text{GaAs}} + y \cdot a_{\text{GaBi}} \quad (4.2)$$

The strain along z-direction is defined by

$$\varepsilon_{\perp} = -\left(\frac{2C_{12}}{C_{11}}\right)\varepsilon_{\parallel} \quad (4.3)$$

where  $C_{11}$  and  $C_{12}$  are the elastic constants of  $\text{GaAs}_{1-y}\text{Bi}_y$ . The strain along the growth direction increases with increasing bismuth concentration and the

strain along x and y-direction increases in negative sense with increasing bismuth concentration. Figures 4.4 gives the corresponding strain values.

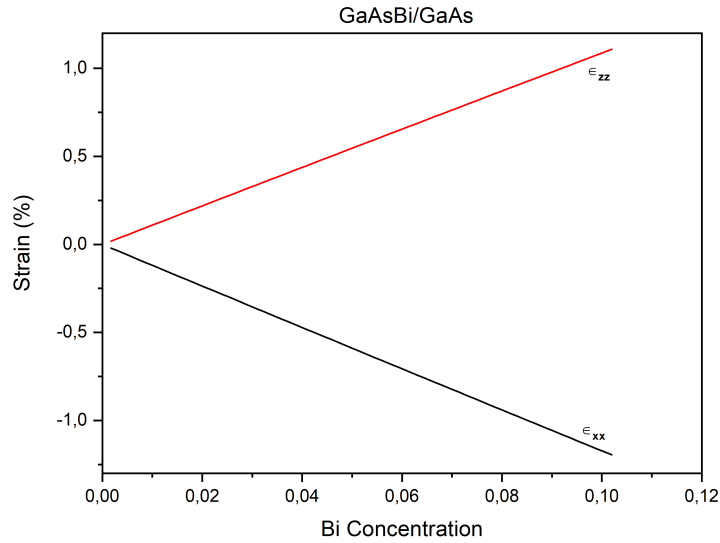


**Figure 4.4** The strain along the growth direction versus bismuth concentration in the  $\text{GaAs}_{1-y}\text{Bi}_y/\text{GaAs}$ .

### 4.3 $\text{GaAs}_{0.94}\text{N}_{0.06}$

III-V GaAs based diluted nitrides systems have been extensively investigated in the last quarter century. When 1 % of As atom is replaced by N in GaAs host material, the  $E_g$  decreases rapidly; by  $\approx 150$  meV [12, 55]. The  $E_g$  reduction in  $\text{GaAs}_{1-x}\text{N}_x$  has been described using C-BAC model due to interaction between the CBE of GaAs host material and the nitrogen impurity energy level [12]. Therefore, the replacement of As atom by N introduces an impurity energy level above the CBE (see Figure 2.1) in a GaAs host material. This is due to the fact that N atom more electronegative and smaller than that of As atom.

Incorporation of a small fraction of nitrogen atom into GaAs host semiconductor material produces dilute nitride alloys leading a  $E_g$  reduction. In GaAsN material, localized impurity nitrogen energy level lies inside the CB. Therefore, we have used C-BAC and provide the results in figure 4.5 showing that the CB splits into two subbands,  $E_+$  and  $E_-$  as a function of N concentration [12].

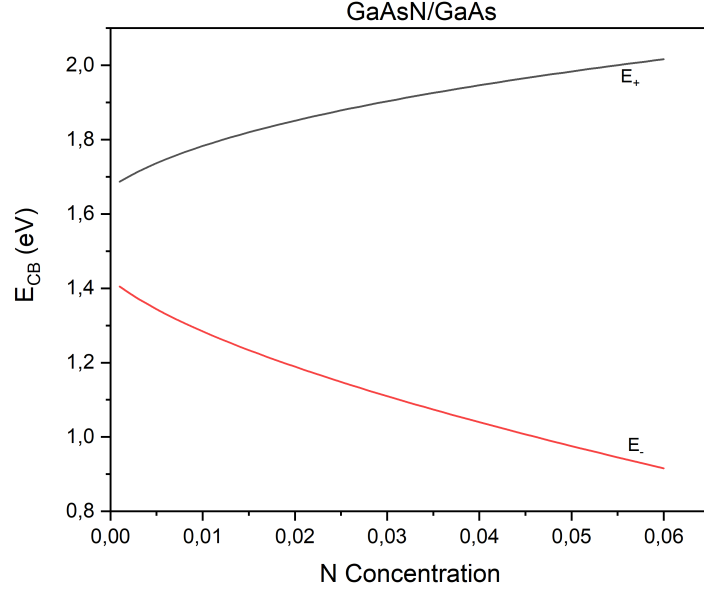


**Figure 4.5** Variation of relative energy positions for  $E_+$  and  $E_-$  as a function of Bi concentration for  $\text{GaAs}_{1-x}\text{N}_x/\text{GaAs}$ .

The in-plane strain for  $\text{GaAs}_{1-x}\text{N}_x/\text{GaAs}$  is defined by

$$\varepsilon_{\parallel} = \frac{a_{\text{GaAs}} - a_{\text{GaAsN}}}{a_{\text{GaAsN}}} \quad (4.4)$$

where  $a_{\text{GaAsN}}$  is the lattice constant of ternary GaAsN material can be calculated by means of using the Vegards law;

$$a_{\text{GaAs}_{1-x}\text{N}_x} = (1 - x) \cdot a_{\text{GaAs}} + x \cdot a_{\text{GaN}} \quad (4.5)$$

The strain along the growth direction is defined by

$$\varepsilon_{\perp} = -\left(\frac{2C_{12}}{C_{11}}\right)\varepsilon_{\parallel} \quad (4.6)$$

where  $C_{11}$  and  $C_{12}$  are the elastic constants of  $\text{GaAs}_{1-x}\text{N}_x$ . The strain along the growth direction increases with an increasing nitrogen concentration and the strain along x and y-direction increases in negative directions with increasing nitrogen concentration. The results of calculated strain values have been given in Figures 4.6.

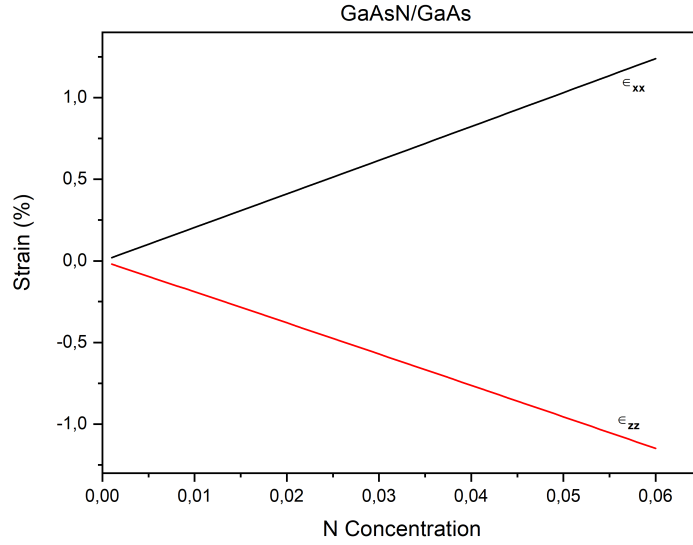


**Figure 4.6** The strain along the growth direction versus nitrogen concentration in the  $\text{GaAs}_{1-x}\text{N}_x/\text{GaAs}$ .

#### 4.4 $\text{GaAs}_{0.82}\text{N}_{0.06}\text{Bi}_{0.12}$

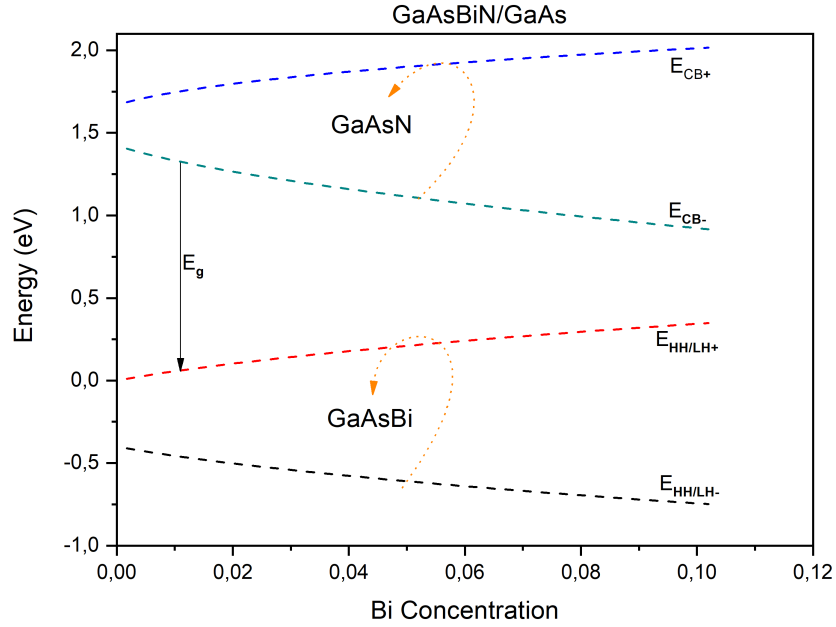
The introduction of Bi into GaAsN produces the GaAsBiN quaternary dilute bismide and nitride alloy. GaAsN on GaAs substrate is tensilely strained heterostructure whereas GaAsBi on GaAs substrate is a compressively strained. Therefore strain values are compensated and can be controlled by means of using the quaternary GaAsBiN alloy. The introduction of N into GaAs results a huge band gap reduction leading an increase in conduction band offset. On the other hand the introduction of Bi into GaAsN increases the VB offset. As a combination of these modifications quaternary dilute nitride bismide alloy of GaAsBiN offers favourable bandstructures for mid-infrared applications with deeper CB and VB offsets, controllable strain values, being  $\Delta_0 > E_g$  and reduced band gap values.

In this section, we extend our model calculations for GaAsBiN including the change in CB and VB due to the presence of Bi and N impurity defect levels. We use the C-BAC and V-BAC models to reveal the composition dependence of band structure of dilute bismide nitride GaAsBiN alloy on GaAs substrates.

Incorporation of both dilute bismide (Bi) and nitride (N) into III-V host materials has attracted great attention due to their interesting band structures. The co-alloying of both N and Bi atoms into GaAs was first proposed by Janotti et al.

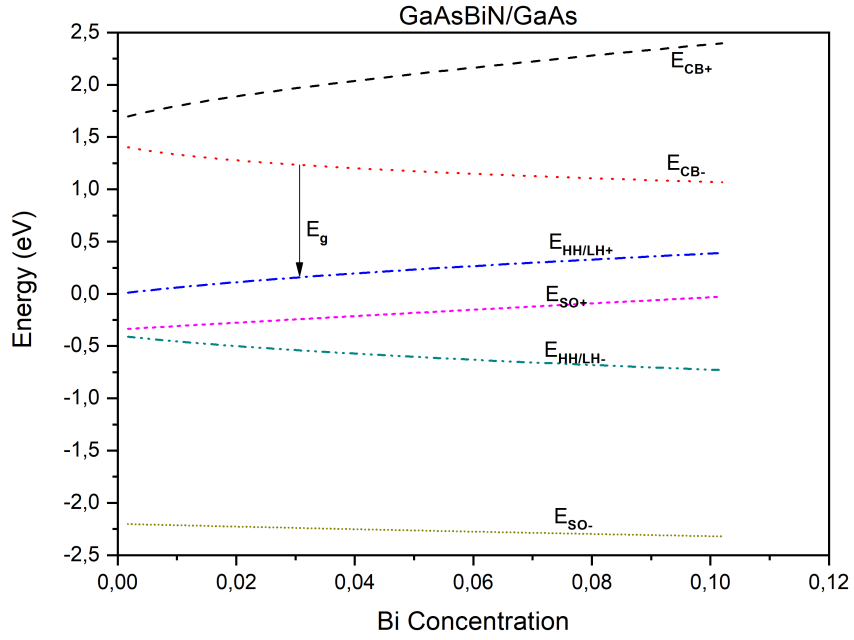


[50]. This kind of co-alloying produces an exotic quaternary material GaAsBiN and allows to control strain and engineer the band structure. Bi mainly affects the VB and N affects the CB. Thus combination of Bi and N atoms in III-V semiconductor alloys offers great potential for engineering the CB and VB offsets [7]. In GaAsBiN material, localized impurity bismuth and nitrogen energy level are introduced into the VB and the CB (see Figure 2.1), respectively. As a result of BAC interaction [12] both VB and CB splits into the conduction subbands, heavy hole, light hole and split-off bands into a series of  $E_+$  and  $E_-$  energy levels. The detailed calculated values of these energy levels is shown in figure 4.7. The  $E_g$  energy can be calculated by means of the energy differences of  $E_g = E_{CB-} - E_{HH/LH+}$  as shown in figure 4.7.



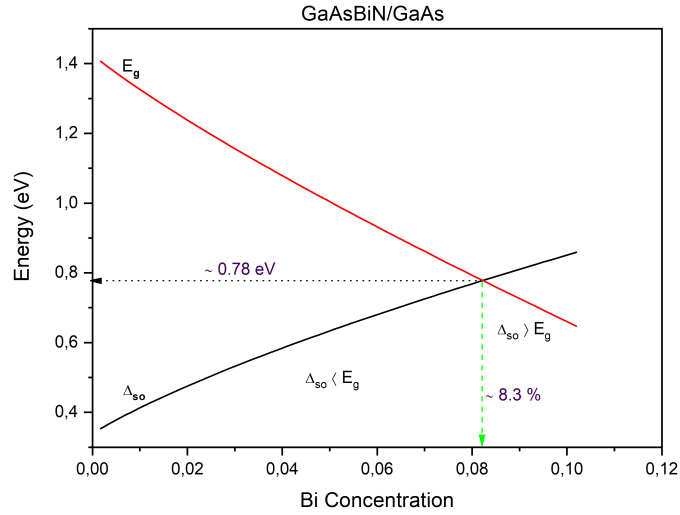
**Figure 4.7** Variation of both  $E_+$  and  $E_-$  levels as a function of Bi (12%) and N (6%) concentration for  $\text{GaAs}_{1-y}\text{Bi}_y/\text{GaAs}$  and  $\text{GaAs}_{1-x}\text{N}_x/\text{GaAs}$ .

Figure 4.8 shows the variations of the conduction band, heavy hole, light hole and split-off bands  $E_+$  and  $E_-$  energy levels with Bi concentration for  $\text{GaAs}_{1-x-y}\text{N}_x\text{Bi}_y$  on GaAs substrate. These variations presented in figure 4.8 illustrates that the  $E_{HH/LH+}$  and  $E_{SO+}$  level increases at the rate of 11.0 meV and 5.5 meV per Bi concentration, however  $E_{CB-}$  level decreases by 17.7 meV.



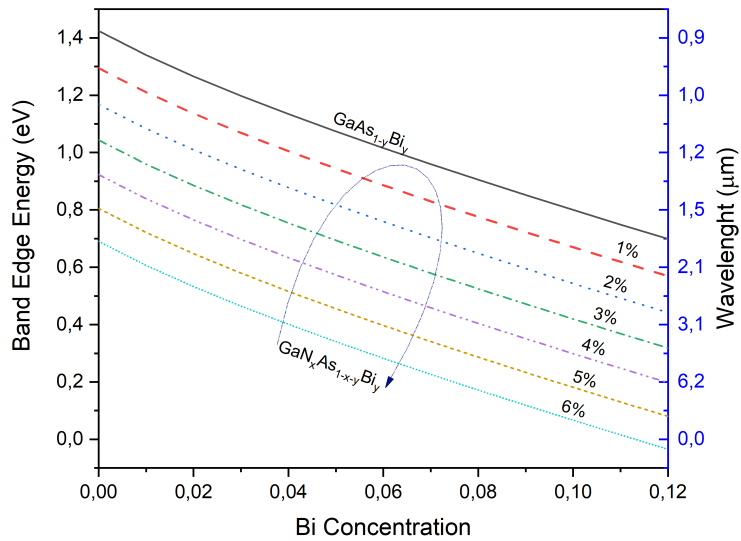
**Figure 4.8** Energy locations  $E_+$  and  $E_-$  of conduction band, heavy hole, light hole and split-off bands for  $\text{GaAs}_{1-x-y}\text{N}_x\text{Bi}_y/\text{GaAs}$  as a function of Bi (12%) and N (6%) concentration.

Figure 4.9 presents the total reduction in  $E_g$  and the rate of change of  $\Delta_0$  as a function of bismide concentration. These variations again show that  $E_g$  and  $\Delta_0$  vary relative to one another with incorporated bismide and nitrogen concentration. As it is seen from figure 4.9, when 8.3 % of bismuth atoms are incorporated, the energy of spin-orbit splitting,  $\Delta_0$  crosses over the band gap energy,  $E_g$  and when bismuth concentration is greater than 8.3 %,  $\Delta_0 > E_g$ . Thus optical loss mechanisms can be eliminated at this value of bismuth (12%) and nitrogen (6%) concentration. Our calculated results that have been illustrated in figure 4.9 shows that band gap decreases by 17.23 meV per Bi concentration, while spin-orbit splitting energy increases  $\approx 13.0$  meV per Bi concentration.



**Figure 4.9** Variation of  $E_g$  and  $\Delta_0$  as a function of Bi (12%) and N (6%) concentration for  $\text{GaAs}_{1-x-y}\text{N}_x\text{Bi}_y/\text{GaAs}$ .

Both nitrogen and bismide affects the  $E_g$  of the host binary GaAs material, but only bismide influences  $\Delta_0$ . To compare the effect of N concentration in  $\text{GaAs}_{1-x-y}\text{N}_x\text{Bi}_y$ , we have considered various concentrations of N (up to 6 %) and the results are given in figure 4.10. Figure 4.11 shows that the strain for  $\text{GaAs}_{1-x-y}\text{N}_x\text{Bi}_y$  is tensile strain while for  $\text{GaAs}_{1-y}\text{Bi}_y$  is a compressive strain.



**Figure 4.10** Estimated variation of band edge energy and wavelength due to Bi (up to 12 %) and N (up to 6 %) incorporation in  $\text{GaAs}_{1-x-y}\text{N}_x\text{Bi}_y/\text{GaAs}$ .

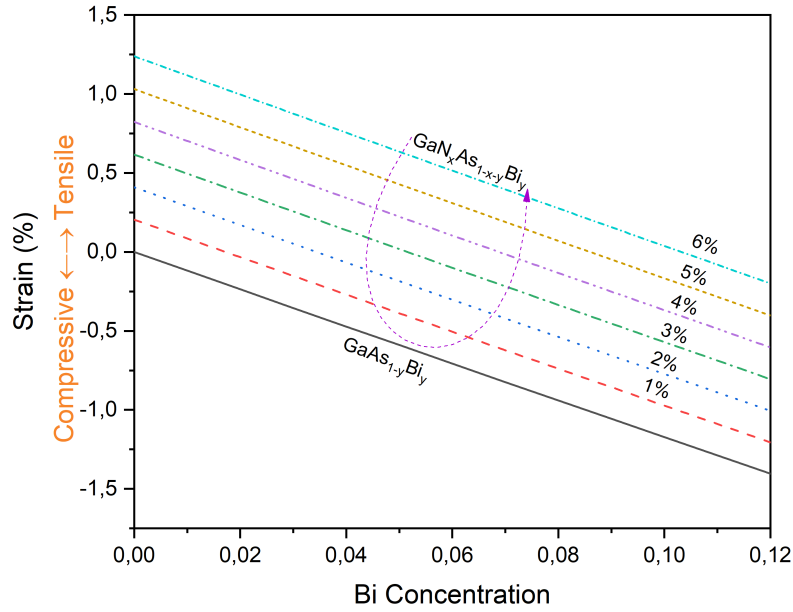


**Figure 4.11** Estimated variation of strain due to Bi (up to 12 %) and N (up to 6 %) incorporation in  $\text{GaAs}_{1-x}\text{N}_x/\text{GaAs}$  and  $\text{GaAs}_{1-y}\text{Bi}_y/\text{GaAs}$ .

#### 4.5 Summary

Our calculated values for GaAsBi alloy on GaAs substrates show that band gap decreases approximately 60 meV/Bi% as stated by Sweeney et al [48]. A band gap value of 800 meV can be reached for a bismuth concentration of  $\approx 9\%$ . This provides an emission wavelength of 1.5  $\mu\text{m}$ . When the bismuth concentration is in the order of 5%, the emission wavelength is  $\approx 1.3 \mu\text{m}$ . The corresponding strain values of these GaAsBi on GaAs substrates are  $\approx 1.2\%$  and  $\approx 0.7\%$  for 9% Bi and 5% Bi, respectively. These results show that GaAsBi ternary alloy system on GaAs provides light emission required in telecommunication with modest strain values. When the Bi concentration is  $\approx 9\%$  in compressive strained GaAsBi layers on GaAs substrates,  $\Delta_0$  becomes greater than  $E_g$ . Thus Auger recombination and IVBA can be eliminated for Bi concentrations being greater than 9% in the near infrared region.

When N and Bi atoms are simultaneously doped into GaAs host material, an exotic quaternary GaAsBiN alloy on a GaAs substrate can be achieved. This material system can be analyzed by means of using C-BAC model for incorporation of dilute nitrides and V-BAC model for incorporation of dilute bismides. Our

calculations shows that  $E_g$  decreases by 17.23 meV per Bi concentration, while  $\Delta_0$  increases in the order of 13.0 meV per Bi concentration. Furthermore, we have shown that the Bi concentration is  $\approx 8.3\%$  in GaAsBiN on GaAs,  $\Delta_0$  becomes greater than  $E_g$ .



## CHAPTER 5

### THESIS SUMMARY AND FUTURE WORK

The work carried out in this thesis is the results of a detailed comparative theoretical analysis of dilute nitride and bismide  $\text{GaN}_{0.06}\text{As}_{0.82}\text{Bi}_{0.12}/\text{GaAs}$  as well as  $\text{InAs}_{0.88}\text{Bi}_{0.12}/\text{GaAs}$ ,  $\text{InP}_{0.88}\text{Bi}_{0.12}/\text{GaAs}$  and  $\text{InSb}_{0.88}\text{Bi}_{0.12}/\text{GaAs}$  alloys. The nitrogen and bismuth concentration dependence of band gap, band edge energy levels and strain and their influence on optical loss mechanism have been investigated. Our calculations are based on the C-BAC model for incorporation of dilute nitrides and the V-BAC model for incorporation of dilute bismides. Thus, the band structure of ternary  $\text{InAs}_{1-x}\text{Bi}_x/\text{GaAs}$ ,  $\text{InP}_{1-x}\text{Bi}_x/\text{GaAs}$ ,  $\text{InSb}_{1-x}\text{Bi}_x/\text{GaAs}$  and  $\text{GaAs}_{1-y}\text{Bi}_y/\text{GaAs}$  materials has been modelled by V-BAC model. On the other hand, C-BAC model has been used for  $\text{GaAs}_{1-x}\text{N}_x/\text{GaAs}$ . Both anti-crossing models have been incorporated for quaternary  $\text{GaN}_x\text{As}_{1-x-y}\text{Bi}_y/\text{GaAs}$  materials. As a result of interaction between extended host band states and localized impurity states, VB states of LH, HH and SO splits into six subbands and CB splits into two subbands with a series of  $E_+$  and  $E_-$  energy levels.  $E_+$  energy level keeps the nature of host alloy whereas  $E_-$  energy level keeps the localized character of impurity states.

Our calculated results show that  $E_g$  decreases with increasing bismuth and nitrogen concentration, while  $\Delta_0$  increases with increasing bismuth concentration which is in agreement with other studies [3, 7–9, 12, 13, 28, 48, 52]. The  $E_g$  and  $\Delta_0$  crosses over at different bismuth and nitrogen concentration for each material system due to their different band properties. We have calculated that  $\Delta_0$  becomes greater than  $E_g$  for  $\approx 0.8\%$ ,  $\approx 48\%$ ,  $\approx 9.7\%$  and  $\approx 8.3\%$  bismuth concentrations for ternary  $\text{InAs}_{1-x}\text{Bi}_x/\text{InAs}$ ,  $\text{InP}_{1-x}\text{Bi}_x/\text{InP}$ ,  $\text{GaAs}_{1-y}\text{Bi}_y/\text{GaAs}$  and quaternary  $\text{GaN}_x\text{As}_{1-x-y}\text{Bi}_y/\text{GaAs}$  materials, respectively. However, there is no need to increase bismuth concentration for  $\text{InSb}_{1-x}\text{Bi}_x$  material system to achieve  $\Delta_0 > E_g$  since it is already satisfied.

When bismuth and nitrogen atoms are incorporated into the host binary material system, there occurs a repulsive interaction between the light hole, heavy-

hole, split-off band and conduction subbands of  $E_+$  and  $E_-$  energy levels due to the localized impurity states that lies inside the VB and the CB edge (see Figure 2.1) of the host material for bismide and nitrogen incorporation respectively. The  $E_{HH/LH+}$  energy level increases at the rate of 32.5, 31.9, 20.8 and 61.5 and the  $E_{SO+}$  energy level increases at the rate of 24.6, 21.7, 24.2, 32.5 meV per Bi incorporation for ternary  $\text{InAs}_{1-x}\text{Bi}_x$ ,  $\text{InP}_{1-x}\text{Bi}_x$ ,  $\text{InSb}_{1-x}\text{Bi}_x$  and  $\text{GaAs}_{1-y}\text{Bi}_y$  materials. The corresponding values are 11.0 and 5.5 meV for quaternary  $\text{GaN}_x\text{As}_{1-x-y}\text{Bi}_y/\text{GaAs}$  materials. We have also shown that  $E_{CB}$  goes in downward direction by increasing bismuth concentration according to virtual crystal approximation. Thus conduction band edge decreases with energy values of 10.3, 17.4, 14.4 and 23.0 meV for ternary  $\text{InAs}_{1-x}\text{Bi}_x/\text{InAs}$ ,  $\text{InP}_{1-x}\text{Bi}_x/\text{InP}$ ,  $\text{InSb}_{1-x}\text{Bi}_x/\text{InSb}$ ,  $\text{GaAs}_{1-y}\text{Bi}_y/\text{GaAs}$  and 17.7 meV for quaternary  $\text{GaN}_x\text{As}_{1-x-y}\text{Bi}_y$  on GaAs materials.

Our calculated results have been shown that the band gap reduction with N concentration is faster in dilute nitrides compared to that of the  $E_g$  reduction with Bi concentration in dilute bismides.

The work carried on this thesis shows that the incorporation of impurity atoms restructure the band structure. Therefore, as a future work, we aim to reveal the consequences of restructuring of valence and conduction bands on the most important loss mechanisms of intervalence band absorption and Auger recombination.

## REFERENCES

- [1] Nathan, M. I., Dumke, W. P., Burns, G., Dill Jr, F. H., Lasher, G. (1962). Stimulated emission of radiation from GaAs p-n junctions. *Applied Physics Letters*. **1**, 62-64.
- [2] Kondow, M., Uomi, K., Niwa, A., Kitatani, T., Watahiki, S., Yazawa, Y. (1996). GaInNAs: A novel material for long-wavelength-range laser diodes with excellent high-temperature performance. *Japanese Journal of Applied Physics*. **35**, 1273-1275.
- [3] Shan, W., Walukiewicz, W., Yu, K. M., Ager Iii, J. W., Haller, E. E., Geisz, J. F., ... Tu, C. W. (2001). Band anticrossing in III-N-V alloys. *Physica Status Solidi (b)*. **223**, 75-85.
- [4] Samajdar, D. P., Dhar, S. (2014). Valence Band Structure of and Alloy Semiconductors Calculated Using Valence Band Anticrossing Model. *The Scientific World Journal*. **2014**.
- [5] Hunter, C.. (2014). Growth and characterization of bulk GaAs<sub>1-x</sub>Bi<sub>x</sub>/GaAs diodes. Ph.D. thesis, University of Sheffield.
- [6] Zhang, Y., Mascarenhas, A., Wang, L. W. (2005). Similar and dissimilar aspects of III-V semiconductors containing Bi versus N. *Physical Review B*. **71**, 155201.
- [7] Sweeney, S. J., Batool, Z., Hild, K., Jin, S. R., Hosea, T. J. C. (2011). The potential role of Bismide alloys in future photonic devices. *In Transparent Optical Networks (ICTON), 2011 13th International Conference on.* (pp. 1-4). IEEE.
- [8] Sweeney, S. J., Jin, S. R. (2013). Bismide-nitride alloys: promising for efficient light emitting devices in the near-and mid-infrared. *Journal of Applied Physics*. **113**, 043110.
- [9] Chai, G. M., Broderick, C. A., O'Reilly, E. P., Othaman, Z., Jin, S. R., Petropoulos, J. P., ... Hosea, T. J. C. (2015). Experimental and modelling study of InGaBiAs/InP alloys with up to 5.8% Bi, and with  $\Delta_0 > E_g$ . *Semiconductor Science and Technology*. **30**. 094015.
- [10] Cheetham, K. J., Krier, A., Marko, I. P., Aldukhayel, A., Sweeney, S. J. (2011). Direct evidence for suppression of Auger recombination in GaInAsSbP/InAs mid-infrared light-emitting diodes. *Applied Physics Letters*. **99**, 141110.



- [11] Broderick C.A., Usman M., O'Reilly E.P. (2013) Theory of the Electronic Structure of Dilute Bismide Alloys: Tight-Binding and  $k \cdot p$  Models. In: Li H., Wang Z. (eds) Bismuth-Containing Compounds. Springer Series in Materials Science, vol 186. Springer, New York, NY.
- [12] Shan W., Walukiewicz W., Ager III J., Haller E., Geisz J., Friedman D., Olson J., Kurtz S.R. (1999). Band anticrossing in GaInNAs alloys. *Physical Review Letters*. **82**, 1221-1224.
- [13] Alberi, K., Dubon, O. D., Walukiewicz, W., Yu, K. M., Bertulis, K., Krotkus, A. (2007). Valence band anticrossing in GaBi<sub>x</sub>As<sub>1-x</sub>. *Applied Physics Letters*. **91**, 051909.
- [14] Wolford D. J., Bradley J. A., Fry K. , Thompson J. 1984. in Proc. of the 17th International Conference on the Physics of Semiconductor, Springer, New York.
- [15] Liu, X., Pistol, M. E., Samuelson, L., Schwetlick, S., Seifert, W. (1990). Nitrogen pair luminescence in GaAs. *Applied Physics Letters*. **56**, 1451-1453.
- [16] Vogl, P. (1984). Predictions of Deep-Impurity-Level Energies. *Advances in Electronics and Electron Physics*. **62**, 101.
- [17] Hjalmarson, H. P., Vogl, P., Wolford, D. J., Dow, J. D. (1980). Theory of substitutional deep traps in covalent semiconductors. *Physical Review Letters*. **44**, 810.
- [18] Schwingenschlgl, U., Chroneos, A., Schuster, C., Grimes, R. W. (2012). Electronegativity and doping in semiconductors. *Journal of Applied Physics*. **112**. 046101.
- [19] Sóllyom, J. (2007). Fundamentals of the Physics of Solids: Volume 1: Structure and Dynamics. (Vol. 1). Springer Science and Business Media.
- [20] Basak, C. B., Sengupta, A. K., Kamath, H. S. (2003). Classical molecular dynamics simulation of UO<sub>2</sub> to predict thermophysical properties. *Journal of Alloys and Compounds*. **360**, 210-216.
- [21] Yuen, H. B. (2006). Growth and characterization of dilute nitride antimonides for long-wavelength optoelectronics. Ph.D. thesis, Stanford University.
- [22] Suemune, I., Uesugi, K., Walukiewicz, W. (2000). Role of nitrogen in the reduced temperature dependence of band-gap energy in GaNAs. *Applied Physics Letters*. **77**, 3021-3023.
- [23] Alberi, K., J., Walukiewicz, W., Yu, K. M., Dubon, O. D., Watkins, S. P., Wang, C.X., Liu, X., Cho, Y.J., Furdyna, J. (2007). Valence-band anticrossing in mismatched III-V semiconductor alloys. *Physical Review B*. **75**, 045203.
- [24] People, R., Sputz, S. K. (1990). Band nonparabolicities in lattice-mismatch-strained bulk semiconductor layers. *Physical Review B*. **41**, 8431.

- [25] Samajdar, D. P., Das, T. D., Dhar, S. (2016). Calculation of Valence Band Structure and Band Dispersion in Indium containing III-V Bismides by k.p method. *Computational Materials Science*. **111**, 497-502.
- [26] Vurgaftman, I., Meyer, J. R., Ram-Mohan L. R. (2001). Band parameters for III-V compound semiconductors and their alloys. *Journal of Applied Physics*. **89**, 5815-5875.
- [27] Vurgaftman I., Meyer J. R. (2003). Band parameters for nitrogen-containing semiconductors. *Journal of Applied Physics*. **94**, 3675-3696.
- [28] Batool, Z., Hild, K., Hosea, T. J. C., Lu, X., Tiedje, T., Sweeney, S. J. (2012). The electronic band structure of GaBiAs/GaAs layers: Influence of strain and band anti-crossing. *Journal of Applied Physics*, **111**, 113108.
- [29] Vegard L. (1921). Die konstitution der mischkristalle und die raumflung der atome. *Zeitschrift fr Physik A Hadrons and Nuclei*. **5 1**, 17-26.
- [30] Bakır, E. (2007). Investigation of the band alignment of long-wavelength InGa(N)As(Sb) quantum wells on GaAs and InP substrates. M.Sc.thesis, University of Gaziantep.
- [31] Chang, C. S., Chuang, S. L. (1995). Modeling of strained quantum-well lasers with spin-orbit coupling. *IEEE Journal of Selected Topics in Quantum Electronics*. **1**, 218-229.
- [32] Okamoto, H., Oe, K. (1998). Growth of metastable alloy InAsBi by low-pressure MOVPE. *Japanese Journal of Applied Physics*. **37**, 1608.
- [33] Kini, R. N., Bhusal, L., Ptak, A. J., France, R., Mascarenhas, A. (2009). Electron hall mobility in GaAsBi. *Journal of Applied Physics*. **106**, 043705.
- [34] Cooke, D. G., Hegmann, F. A., Young, E. C., Tiedje, T. (2006). Electron mobility in dilute GaAs bismide and nitride alloys measured by time-resolved terahertz spectroscopy. *Applied Physics Letters*. **89**, 122103.
- [35] Das, T. D. (2014). The effect of Bi composition on the properties of InP<sub>1-x</sub>Bi<sub>x</sub> grown by liquid phase epitaxy. *Journal of Applied Physics*. **115**, 173107.
- [36] Sandall, I. C., Bastiman, F., White, B., Richards, R., Mendes, D., David, J. P. R., Tan, C. H. (2014). Demonstration of InAsBi photoresponse beyond 3.5  $\mu$ m. *Applied Physics Letters*. **104**, 171109.
- [37] Marko, I. P., Ludewig, P., Bushell, Z. L., Jin, S. R., Hild, K., Batool, Z., ... Sweeney, S. J. (2014). Physical properties and optimization of GaBiAs/(Al) GaAs based near-infrared laser diodes grown by MOVPE with up to 4.4% Bi. *Journal of Physics D: Applied Physics*. **47**, 345103.
- [38] Barnett, S. A. (1987). Direct E<sub>0</sub> energy gaps of bismuth-containing III-V alloys predicted using quantum dielectric theory. *Journal of Vacuum Science and Technology A: Vacuum, Surfaces, and Films*. **5**, 2845-2848.

- [39] Carrier, P., Wei, S. H. (2004). Calculated spin-orbit splitting of all diamondlike and zinc-blende semiconductors: Effects of p 1/2 local orbitals and chemical trends. *Physical Review B*. **70**, 035212.
- [40] Streubel, K., Linder, N., Wirth, R., Jaeger, A. (2002). High brightness Al-GaInP light-emitting diodes. *IEEE Journal of Selected Topics in Quantum Electronics*. **8**, 321-332.
- [41] Yamamoto, M., Yamamoto, N., Nakano, J. (1994). MOVPE growth of strained InAsP/InGaAsP quantum-well structures for low-threshold 1.3- $\mu\text{m}$  lasers. *IEEE Journal of Quantum Electronics*. **30**, 554-561.
- [42] Berding, M. A., Sher, A., Chen, A. B., Miller, W. E. (1988). Structural properties of bismuth-bearing semiconductor alloys. *Journal of Applied Physics*. **63**, 107-115.
- [43] Dimroth, F., Howard, A., Shurtleff, J. K., Stringfellow, G. B. (2002). Influence of Sb, Bi, Tl, and B on the incorporation of N in GaAs. *Journal of Applied Physics*. **91**, 3687-3692.
- [44] Tominaga, Y., Kinoshita, Y., Oe, K., Yoshimoto, M. (2008). Structural investigation of GaAs<sub>1-x</sub>Bi<sub>x</sub>/GaAs multiquantum wells. *Applied Physics Letters*. **93**, 131915.
- [45] Lewis, R. B., Beaton, D. A., Lu, X., Tiedje, T. (2009). GaAs<sub>1-x</sub>Bi<sub>x</sub> light emitting diodes. *Journal of Crystal Growth*. **311**, 1872-1875.
- [46] Asbeck, P. M., Welty, R. J., Tu, C. W., Xin, H. P., Welser, R. E. (2002). Heterojunction bipolar transistors implemented with GaInNAs materials. *Semiconductor Science and Technology*. **17**, 898.
- [47] Fluegel, B., Francoeur, S., Mascarenhas, A., Tixier, S., Young, E. C., Tiedje, T. (2006). Giant spin-orbit bowing in GaAs<sub>1-x</sub>Bi<sub>x</sub>. *Physical Review Letters*. **97**, 067205.
- [48] Sweeney, S. J. (2010). Bismide-alloys for higher efficiency infrared semiconductor lasers. In *Semiconductor Laser Conference (ISLC), 2010 22nd IEEE International* (pp. 111-112). IEEE.
- [49] Oe, K., Okamoto, H. (1998). New semiconductor alloy GaAs<sub>1-x</sub>Bi<sub>x</sub> grown by metal organic vapor phase epitaxy. *Japanese Journal of Applied Physics*. **37**, L1283.
- [50] Janotti A., Wei S. H., Zhang S. B. (2002). Theoretical study of the effects of isovalent coalloying of Bi and N in GaAs. *Physical Review B*. **65**, 115203.
- [51] Wu, J., Shan, W., Walukiewicz, W. (2002). Band anticrossing in highly mismatched III-V semiconductor alloys. *Semiconductor Science and Technology*. **17**, 860.
- [52] O'Reilly, E. P., Lindsay, A., Fahy, S. (2004). Theory of the electronic structure of dilute nitride alloys: beyond the band-anti-crossing model. *Journal of Physics: Condensed Matter*. **16**, S3257.

- [53] Usman, M., Broderick, C. A., Batool, Z., Hild, K., Hosea, T. J., Sweeney, S. J., O'Reilly, E. P. (2013). Impact of alloy disorder on the band structure of compressively strained  $\text{GaBi}_x\text{As}_{1-x}$ . *Physical Review B*. **87**, 115104.
- [54] Usman, M., Broderick, C. A., Lindsay, A., O'Reilly, E. P. (2011). Tight-binding analysis of the electronic structure of dilute bismide alloys of GaP and GaAs. *Physical Review B*. **84**, 245202.
- [55] Lindsay, A., O'Reilly, E. P. (1999). Theory of enhanced bandgap non-parabolicity in  $\text{GaN}_x\text{As}_{1-x}$  and related alloys. *Solid state communications*. **112**, 443-447.

